A numerical study of the subgrid-scale fluid motion in turbulent flows

by

© Mohammed Khalid Hossen
B. Sc.(Hons), MSc.

A thesis submitted to the
School of Graduate Studies
in partial fulfillment of the
requirements for the degree of
Masters of Science.

Department of Scientific Computing
Memorial University of Newfoundland

October 13, 2021

ST. JOHN'S NEWFOUNDLAND

Abstract

The numerical solution of the Navier–Stokes equations for different turbulence regimes has become more prevalent for many years. This thesis has investigated the large eddy simulation method for solving the Navier–Stokes equations. A primary goal is to design a subgrid-scale model for small-scale coherent vortices while statistically maintaining an accurate dissipation rate. Past investigations of turbulence indicate that the vortex stretching mechanism can transport the turbulence kinetic energy from large to small scales. Thus, a turbulence model can learn the energy dissipation rate from the statistics of the velocity gradient tensor. Following such a hypothesis, this thesis validates how vortex stretching can directly account for the subgrid-scale dissipation rate while solving the Navier–Stokes equations on a relatively coarse mesh. Current findings suggest a potential subgrid-scale model based on invariants of the square of the velocity gradient tensor. The turbulence statistics obtained from the proposed model agree well with the three commonly used dynamically adaptive large eddy simulation techniques. The results also suggest that statistics of the velocity gradient tensor dynamically adapt the dissipation rate to the local variation of turbulence. Furthermore, considering the square of the deformation tensor, this thesis suggests that the singular values of the snapshots of the velocity gradient may improve the model in future studies of more challenging turbulent flows.

Statement of Contribution

This manuscript-based thesis presents a numerical study of the subgrid-scale motion in turbulent flows. In this approach, the LES method is developed to solve the Navier–Stokes equations to resolve the large-scale flows, while the subgrid-scale models are required to model the unresolved scales of motion to the resolved scales. This thesis mainly focuses on these two topics. Topic 1 is the design of a vortex-stretching-based subgrid-scale model in LES, and topic 2 is the statistical analysis of the turbulence modeling. The work of this thesis is also divided into two stages such as data collection and statistical analysis. All of the simulated data are available for further research of data-driven turbulence modeling.

Mohammed Khalid Hossen (MKH) wrote this thesis with the help and guidance of Jahrul Alam (JA) and Asokan Variyath (AV). The contributions of each co-author have been listed below.

Contribution	Topic 1	Topic 2
Research proposal	JA and AV	JA and AV
Literature review	MKH	MKH
Statistical Methodology	JA and AV	JA and AV
Simulation, data collection, analysis	MKH	MKH
Preparation of chapter	MKH	MKH
Data availability	MKH	MKH
Status	Working paper (chapter 2)	published (chapter 3)

Acknowledgments

In the first place, I would like to thank my supervisor, Dr. Jahrul Alam, and Dr. Asokan Variyath for their consistent support, inspiration, and encouragement to explore new ideas throughout my study at the Memorial University of Newfoundland (MUN). I want to express my gratitude to the School of Graduate Studies at the Memorial University of Newfoundland. I am grateful to the Department of Computer Science and Engineering at Sylhet Agricultural University, Bangladesh, for granting me a paid leave for the entire period of my studies in Canada.

I would also like to thank the chair of the Scientific Computing discipline at the Memorial University of Newfoundland and Compute Canada for high-performance computing support. I am grateful to all the members of our research group, faculty, staff, or other students at the Memorial University of Newfoundland who contributed to my learning. I like to thank specially to Jagdeep Singh for his help and support.

Finally, I am grateful to my wife, Dr. Jannatul Ferdaus, and my parents (S. M. Ashraf Uddin and Khaleda Begum) for their love and support all time.

Contents

List of Tables

List of Figures

List of Symbols

M	Number of realizations
$\bar{u_i}$	Resolved velocity
Δt	Time step
Δ	Cutoff length
δ_{ij}	Kronecker delta
Δ_{les}	Computational grid size
ϵ	Viscous dissipation rate
η	Kolmogorov length scale
λ	Taylor microscale
$\lambda_1, \lambda_2, \lambda_3$	Eigenvalues of strain tensor
$\langle \epsilon \rangle$	Average viscous dissipation rate
$\langle \tau_{ij} \mathcal{S}_{ij} \rangle$	The energy flux
$\langle u_i \rangle$	Mean velocity
$\langle u_i' u_j' \rangle$	Reynolds stress tensor
$\mathcal{G}$	Velocity gradient tensor
$\mathcal{N}$	Number of computational cells
$\mathcal{X}$	A data matrix

$\mathcal{R}e_\lambda$ Taylor Reynolds number

$\mathcal{S}\boldsymbol{\omega}$ Vortex stretching vector

$\mathcal{S}_{ij}$ Strain rate of tensor

$\mathcal{S}_{ij}\mathcal{S}_{ij}$ Total strain production

$\mathcal{S}_{ij}\mathcal{S}_{jk}\mathcal{S}_{ki}$ Self-amplification rate

$\mathcal{S}^d_{ij}$ Traceless symmetric part of the square of the velocity gradient tensor

ν Kinematic viscosity

ν_τ Subgrid-scale viscosity

Ω Computational domain size

ω_i Vorticity vector

$\omega_i\omega_j\mathcal{S}_{ij}$ Enstrophy Production via vortex stretching

τ_{ii} Trace of the residual stress

τ_{ij} Subfilter stress tensor

C_e Constant for turbulence model

C_k Constant for turbulence model

C_s Constant for Smagorinsky model

C_w Constant for turbulence model SGS-A

D Discriminant line

dE/dt The rate of change of the resolved energy

$E(0)$ Initial resolved kinetic energy

$E(k)$ Energy spectrum

$E(t)$ Resolved kinetic energy

f_i	The external body force
k_{sgs}	Turbulent kinetic energy
L	Characteristics length scale
Q_G	Second invariant of the velocity gradient tensor
Q_R	Second invariant rotation rate
Q_S	Second invariant strain rate
R_G	Third invariant of the velocity gradient tensor
R_S	Third invariant strain rate
R_{ij}	Rotation rate of tensor
S_0	Skewness
t	Time
t/T	Dimensionless eddy-turn over time
t_0	Initial time
Tr	Trace
u_i	Instantaneous velocity
u_i'	Fluctuated velocity
u_{rms}	RMS velocity
x_i	The Cartesian coordinate system

List of Abbreviations

NSE Navier-Stokes equation

WALE Wall-Adaptive Local viscosity model

SGS Subgrid-scale

HIT Homogeneous isotropic turbulence

SGS-A WALE model

SGS-B Localized dynamic kinetic energy model

SGS-C TKE-based model

SGS-D Lagrangian dynamic model

DNS Direct Numerical Simulation

RANS Reynolds-Average Navier-Stokes

LES Large Eddy Simulation

PISO Pressure-Implicit with Splitting of Operators

TKE Turbulent kinetic energy

JPDF Joint probability density function

Chapter 1

Introduction

1.1 Turbulent flow

Turbulent flow is a common phenomenon observed in the ocean, atmosphere, and many engineering applications. Airflow around cars, buildings, airplanes, and currents in the ocean, etc., are examples of a turbulent flow (Kundu et al., 2008). Generally, fluid motion can be classified into laminar and turbulent flows. When the flow is smooth and regular, it's known as laminar flow, see Fig. 1.1. In comparison, turbulent flows are characterized by the strong fluctuation of physical properties in space and time, see Fig. 1.1, where instantaneous velocity can be decomposed into the mean and fluctuating components. However, a fluctuating motion does not always lead to turbulent flow, as in the example of gravity waves in the ocean that can fluctuate without turbulence, and in the instance of wind-driven ocean-surface waves creating a fluctuating motion that is not turbulent (Kundu et al., 2008). So, it is a complex task to define turbulent flows precisely. Nevertheless, turbulent flows can be generalized based on their characteristics (Davidson, 2004; Kundu et al., 2008). The main characteristics of turbulent flows are:

- Three-dimensional and rotational.
- Highly unsteady
- Vorticity
- Dissipative
- Broad spectrum of length and time scales

Turbulent flow is three-dimensional because flow parameters like velocity, pressure, etc., vary in the three coordinate directions. However, turbulent flows are much different in three-dimension (3D). The main reason is that vortices stretch other vortices by vortex stretching mechanism in 3D. On the other hand, vortices only move others around without changing strength in two-dimension (2D) because the vortex stretching mechanism is not presented in 2D phenomena.

Turbulent flow refers to an irregular motion of a gas or a liquid. Such a fluid motion occurs around us, which can influence our day-to-day activities. For instance, from 1980 to 2008, 234 turbulence-related incidents were reported, causing a loss of millions of dollars (Storer, Williams, & Gill, 2019). For example, 298 passengers got serious injuries and three fatalities on the United States operated air carriers in that period. The drag coefficient mainly measures the performance of aerodynamics effects on a vehicle, and it can be seen that turbulence has a direct impact on the fuel consumption of commercial and domestic use vehicles (Verzicco et al., 2002). The investigation of such processes will reveal the various ways turbulence affects everyday lives and industry, providing ample opportunities to save millions of dollars.

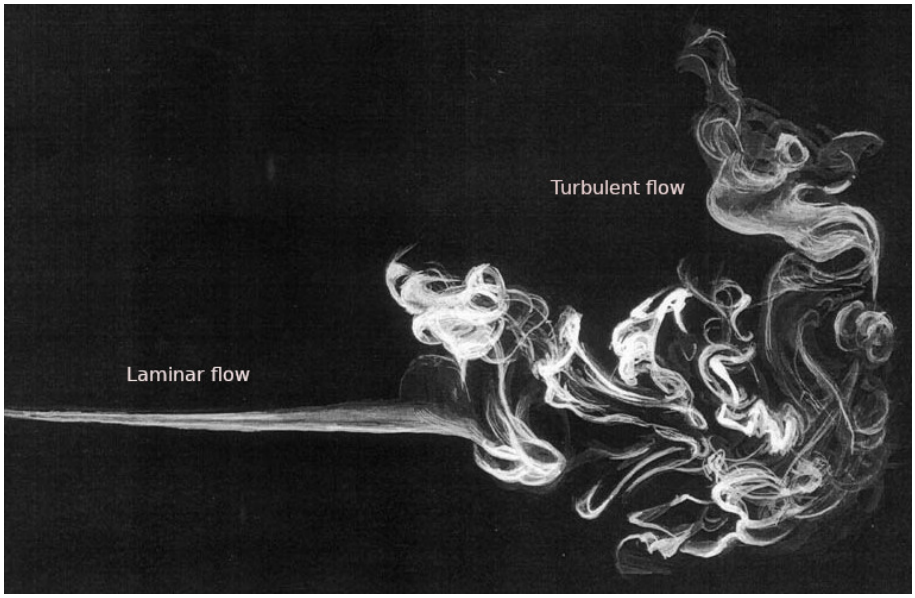

Figure 1.1: A schematic representation of laminar and turbulent flow. Source: Davidson (2004).

Researchers have been studying the turbulent flows through the analytical theories (Kolmogorov, 1941), experiments (Reynolds, 1883), and numerical simulations since the 19^{th} century (Tennekes & Lumley, 2018). Nevertheless, until now, the problem of turbulent flows is still a mystery. The Navier–Stokes equations (NSE) governs the fluid motion, whether applied to laminar or turbulent flows. In particular, the time-dependent, three-dimensional Navier-Stokes equation describes the physics

of turbulent flows. However, most of the engineering applications find it extremely expensive to resolve the entire range of spatial and temporal scales of turbulent flow due to the non-linearity of the advection term (Wilcox et al., 1998). Therefore, the aims of turbulence modeling are to develop an approximate solution to the Navier–Stokes equations in such a way that it either represents turbulence in terms of mean properties or that minimizes the spatial or temporal resolution requirements of the model. Before discussing the methodology of turbulence modeling, the following section covers the related literature review that refers to the motivation for and objective of this thesis.

1.2 Motivation and overall objectives

We can develop rigorous mathematical models for subgrid-scale turbulence if we fully understand how to connect turbulence dissipation with vortex stretching. Thus, following the pioneering work of (Taylor, 1932), this thesis plans to study the role of vortex stretching in the turbulence energy cascade. It is worth mentioning that the energy cascade usually occurs through a hierarchical process of instabilities whereby eddies break down and pass their energy from larger to smaller eddies to even smaller eddies, where the energy is dominated by viscous diffusion (Richardson, 2007). This idea is known as Richardson's hypothesis. The objectives of the thesis stem from two facts. First, it is difficult to describe an apparent mathematical connection between the break-down of eddies and the Navier–Stokes equations (NSE) (Kevlahan et al., 2007). Second, turbulence is not space-filling, which means that small-scale eddies are highly intermittent in space (J. Alam & Islam, 2015). Therefore, there is a need to understand how adequately we can model the inhomogeneous distribution of subgrid-scale energy distribution if the subgrid-scale eddy viscosity comes through the vortex stretching mechanism.

More specifically, the velocity gradient tensor allows for vortex stretching, and thus, it appears directly in the Navier–Stokes equations. Therefore, knowing how to model subgrid-scale turbulence with the square of the velocity gradient tensor via vortex stretching will help us find the energy cascade. Hence, this study investigates a dynamic approach to the subgrid-scale turbulence modeling, where the dissipation process through the second invariant of the squared velocity gradient tensor is defined. For this study, the best strategy is to compare the results among representative other dynamic turbulence models. The standard statistical techniques are also considered to understand the performance of the models quantitatively.

Mathematically, the goal is to lay a functional dependence between the subgrid-scale stress tensor τ_{ij} and the velocity gradient tensor, namely, $\tau_{ij} = \mathcal{F}(\frac{\partial u_i}{\partial x_j})$. Since τ_{ij} is not known, this thesis is not in a position to find $\mathcal{F}$ as an inverse problem via an optimization algorithm. Rather, it wants to define $\mathcal{F}$ in a way that subgrid-scale dissipation is optimized at least at grid-scale turbulence. Moreover, we need to ensure that the model preserves some geometric structure of turbulence. Following this, the joint probability density function of the invariants of the velocity gradient tensor has been studied. A potentially novel aspect of the development is that this thesis can predict the subgrid-scale stress τ_{ij} by this method using an appropriately filtered velocity gradient tensor and improve it dynamically by finding $\mathcal{F}$ through an optimization method.

Hence, the thesis's primary goal is to study how a subgrid-scale turbulence model could extract necessary information about the subgrid-scale dissipation. The study of *a posteriori* statistics of the large eddy simulation (LES) results of four subgrid-scale models provides essential knowledge on the statistics of the velocity gradient tensor to reach the overall objectives stated above. The research of the present thesis is studied in two stages. First, a parallelized LES code is developed that associates vortex stretching in the subgrid-scale model (Nicoud & Ducros, 1999; Trias et al., 2015). For understanding the role of vortex stretching, the first- and higher-order moment of *a posteriori* statistics of LES results are compared among the subgrid-scale models (Fureby et al., 1997). Second, the joint probability density function (JPDF) of invariants of the velocity gradient is studied for understanding the physics of vortex stretching, and the dissipation of subgrid-scale energy in the subgrid-scale models (Martín & Dopazo, 1995; da Silva & Pereira, 2008). In the next section, the thesis outline is presented as follows.

1.3 Outline of the thesis

The thesis is structured as follows. Chapter 2 presents a review of the supporting information of relevant mathematical properties, a methodology of large eddy simulation including the filtering operation and subgrid-scale models, and the statistics of velocity and its gradient tensor. In this chapter, the preliminary results discussed are intended to serve as the basis for the statistical analysis. In Chapter 3, the statistical analysis of the role of vortex stretching in LES has been discussed. Finally, the last Chapter 4 describes a discussion and conclusion of the thesis as well as directions for future work.

Chapter 2

Theoretical background

The first two sections of this chapter cover a preliminary review that offers introductory descriptions of the incompressible Navier–Stokes equations, vorticity, vortex stretching, energy cascade, and velocity gradient tensor to define the mathematical terminology, notations, and physical meaning in this thesis. In Section 2.3, the large eddy simulation and the statistics of velocity and its gradient are briefly discussed. Finally, some primary numerical results are shown in Section 2.4.

2.1 Navier-Stokes equations

The governing equation of continuity and the Navier–Stokes equations (NSE) for an incompressible flow can be written by:

$$\frac{\partial u_i}{\partial x_i} = 0, \tag{2.1}$$

$$\frac{\partial u_i}{\partial t} + u_j \frac{\partial u_i}{\partial x_j} = -\frac{1}{\rho}\frac{\partial P}{\partial x_i} + \nu \frac{\partial^2 u_i}{\partial x_j \partial x_j}, \tag{2.2}$$

where u_i is the ith velocity component, $\boldsymbol{u} = (u_1, u_2, u_3)$ is the velocity vector, and $\boldsymbol{x} = (x_1, x_2, x_3)$ is the Cartesian coordinate system. Here, ρ is the constant density, P is the pressure field, and ν is the kinematic viscosity. We must also add the initial and boundary conditions to this system in order to create a well-posed problem. For example, the boundary condition is periodic for the velocity $\boldsymbol{u}$ and the initial condition is $\boldsymbol{u} = \boldsymbol{u}_0$ at time $t = 0$ to this system in a domain $\Omega = [0, 2\pi]^3$.

2.2 Some mathematical properties

Turbulent flows are rotational and are characterized by high fluctuating vorticity (Kundu et al., 2008). This section discusses the vortex stretching mechanism in the vorticity transport equation and the implications for turbulent flow dynamics. After that, this discussion will include a review of the foundational information for energy cascade and Kolmogorov's similarity hypothesis as they pertain to the role of vortex stretching.

2.2.1 Vorticity, vortex line, and vortex tubes

If we take a curl of the velocity vector $\boldsymbol{u}$, we obtain the vorticity field, say $\boldsymbol{\omega} = \nabla \times \boldsymbol{u}$, where $\boldsymbol{\omega}$ is the vorticity vector. In general, it is a vector field that gives a measure of local rotaion of fluid percels. A connected fluid region with a high concentration of co-directional (or nearly co-directional) vorticity is known as a vortex, such as a tornado or a whirlpool. Vortices are a major component of turbulent flow. Vortices are defined by their velocity distribution, vorticity, and the idea of circulation. The fluid flow velocity in most vortices is significant near the axis and decreases in inverse proportion to the distance from the axis. Vortices have the ability to stretch, twist, and interact in a variety of ways. However, angular and linear motion, energy, and mass are all carried by a moving vortex. A vortex line (like a streamline of the velocity vector) is a curve in the fluid flow where the vorticity is tangent at each point to the line. The vortex lines are parallel to the vorticity vector at each point, while the vortex tube is a cylindrical shape in space where the surface elements are composed of vortex lines, see (Kundu et al., 2008; Tennekes & Lumley, 2018).

2.2.2 Vorticity dynamics

By taking a curl of the equation 2.2, the equation for the transport of vorticity is obtained by:

$$\frac{\partial \omega_i}{\partial t} + u_j \frac{\partial \omega_i}{\partial x_j} = \omega_j \mathcal{S}_{ij} + \nu \frac{\partial^2 \omega_i}{\partial x_j \partial x_j}, \tag{2.3}$$

where the equation 2.3 illustrates the dynamics and generation of vorticity in the three-dimensional turbulent flow (Tennekes & Lumley, 2018). The term $u_j \frac{\partial \omega_i}{\partial x_j}$ on the left-hand side of equation 2.3 indicates the effects of the expansion of the vorticity field. The last term $\nu \frac{\partial^2 \omega_i}{\partial x_j \partial x_j}$ is represented as the vortex destruction on the vorticity distribution field. The quantity $\mathcal{S}_{ij} = \frac{1}{2}\left(\frac{\partial u_i}{\partial x_j} + \frac{\partial u_j}{\partial x_i}\right)$ is the rate of strain tensor and the term $\omega_j \mathcal{S}_{ij}$ on the right-hand side is called the vortex stretching term. This

vortex stretching term is often regarded as the most important mechanism in turbulence dynamics, which refers to the interaction between the vorticity and the strain rate. This term shows some basic differences between the two- and three-dimensional turbulent flows. However, the three-dimensional turbulent flow is the main focus of this thesis.

In two-dimensional flow, the velocity has the component $u_i = (u, v, 0)$ which implies that the vortex stretching term vanishes ($\omega_j \mathcal{S}_{ij} = 0$) because only the z-direction has a nonzero component of vorticity, $\omega_i = (0, 0, \omega_z)$, and thus, it has no effect on the evolution of vorticity field. On the other hand, for three-dimensional flow, this mechanism represents the increment of the vorticity field by stretching, compressing, tilting, and transferring the turbulent energy from large eddies to small eddies. So, vortex stretching is a mechanism in a turbulent flow in which vorticity is amplified by stretched fluid elements to conserve the angular momentum (Tennekes & Lumley, 2018). It suggests that the vortex stretching mechanism is thought to be responsible for local vorticity amplification. As a result, the development of smaller and smaller-scale eddies is generated in the flow field. This procedure indicates a transfer of energy from large to smaller eddies, which is commonly referred to as the energy cascade.

2.2.3 Energy cascade

Classic theories for the cascade in turbulent flows explain how the energy is transferred among these scales. Whether the cascade is towards the smaller scales (forward cascade) or to the larger scales (backward cascade) depends on the type of the flow. It is well verified through experimental and numerical studies that in three-dimensional homogenous isotropic turbulence, on average, energy is transferred from the large to small scales called the forward cascade. In 1941 Kolmogorov quantified this theory and presented two popular hypotheses, which are explained in the following discussion (Kolmogorov, 1941).

First similarity hypothesis: The first similarity hypothesis of Kolmogorov is that the small scales motion statistics have a universal form at a sufficiently high Reynolds number, which describes an independent type of flow that is determined by two parameters only: the rate of dissipation (ϵ); and the kinematic viscosity ν. The length of small scales at which the viscosity acts to dissipate the energy is called the Kolmogorov scale, which is denoted by η (Pope, 2001).

Second similarity hypothesis: The second similarity hypothesis is that the statistics of motion

in a range $l_0 >> l >> \eta$ have a universal form at a sufficiently high Reynolds number, where the motion depends on only the rate of dissipation (ϵ) but in a state that is independent of viscosity (ν), see Fig. 2.2(a). In this hypothesis, universal statistics of motions regime the inertial subrange, see Fig. 2.2(b) (Pope, 2001).

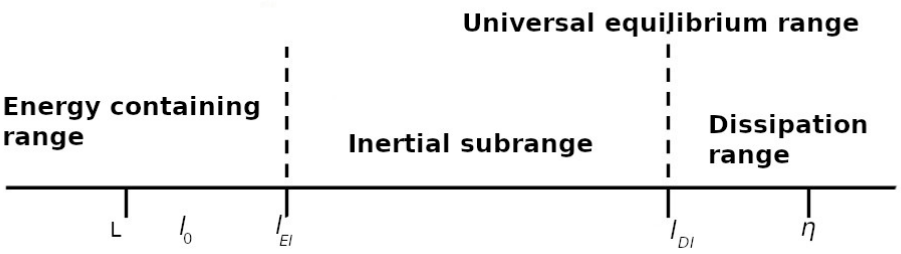

Figure 2.1: Schematically representation of the range of scales of energy. Source: Pope (2001).

The distribution of turbulent kinetic energy among the various sizes of scales is needed to be determined. It is commonly accomplished by looking at the energy spectrum (Pope, 2001). The energy spectrum contains the eddy size of L corresponding to the wavenumber k, which is defined by $k = 2\pi/L$. Now, the kinetic energy and dissipation rate in the wavenumber range (k_a, k_b) is defined by:

$$k_{(k_a,k_b)} = \int_{k_a}^{k_b} E(k)dk,$$
$$\epsilon_{(k_a,k_b)} = \int_{k_a}^{k_b} 2\nu k^2 E(k)dk,$$

where k_a and k_b are the minimum and maximum wavenumber, respectively. In the second similarity hypothesis, the energy spectrum $E(k)$ depends on the wavenumber (k) and the energy dissipation rate (ϵ) in the inertial subrange. Now, based on the concept of dimensional analysis, we found that the kinetic energy $E(k) = C_k k^\alpha \ \epsilon^\beta$, where C_k is constant and

$$[E] = m^3/s^2,$$
$$[k] = 1/m,$$
$$[\epsilon] = m^2/s^3.$$

After simplification the above dimensions, we get $m^3 = m^{-\alpha} m^{2\beta}$. So, $-\alpha + 2\beta = 3$. Besides, $s^{-2} = s^{-3\beta}$. So, $-3\beta = -2$. Now, we obtain the kinetic energy for α and β as $E(k) = C_k \epsilon^{2/3} k^{-5/3}$

(Pope, 2001), where $C_k = 1.5$ is the universal Kolmogorov constant. It is known as the famous Kolmogorov $-5/3$ spectrum, see 2.2(b) (Kolmogorov, 1941):

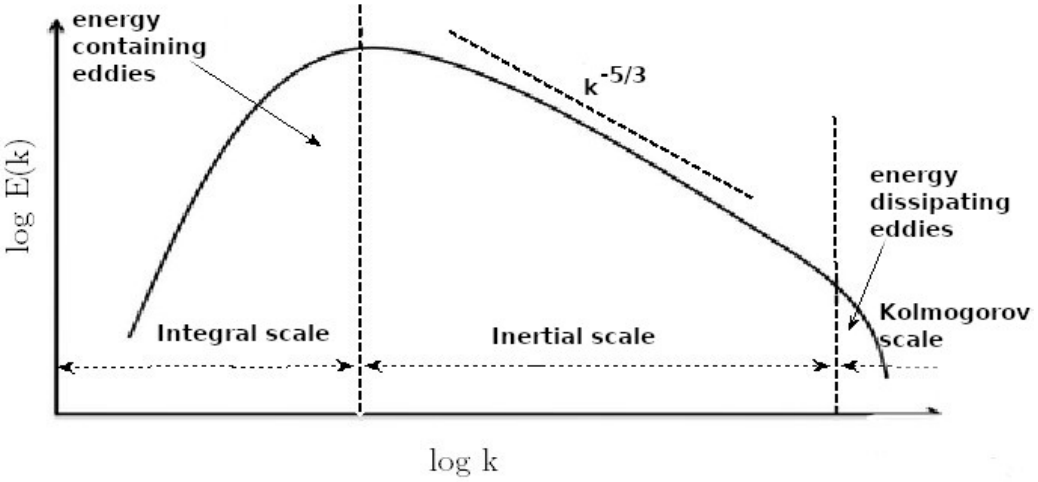

Figure 2.2: Schematically representation of the energy spectrum cascade of a turbulent flow. Source: Pope (2001).

2.2.4 Velocity gradient tensor

In this study, the velocity gradient tensor is defined by $\frac{\partial u_i}{\partial x_j}$, which is the second-order tensor of nine elements that can be written as:

$$\frac{\partial u_i}{\partial x_j} = \begin{pmatrix} \frac{\partial u}{\partial x} & \frac{\partial u}{\partial y} & \frac{\partial u}{\partial z} \\ \frac{\partial v}{\partial x} & \frac{\partial v}{\partial y} & \frac{\partial v}{\partial z} \\ \frac{\partial w}{\partial x} & \frac{\partial w}{\partial y} & \frac{\partial w}{\partial z} \end{pmatrix} = \frac{1}{2}\left(\frac{\partial u_i}{\partial x_j} + \frac{\partial u_j}{\partial x_i}\right) + \frac{1}{2}\left(\frac{\partial u_i}{\partial x_j} - \frac{\partial u_j}{\partial x_i}\right),$$

Where u, v, and w represent the velocity component of the velocity vector and x, y, and z are the Cartesian coordinates axis. The velocity gradient tensor is decomposed into the rate of strain, $\frac{1}{2}\left(\frac{\partial u_i}{\partial x_j} + \frac{\partial u_j}{\partial x_i}\right)$ (symmetrical part), and the rate of rotation $\frac{1}{2}\left(\frac{\partial u_i}{\partial x_j} - \frac{\partial u_j}{\partial x_i}\right)$ (anti-symmetric part). Hence, the effect of stretching is related to the rate of strain of the velocity gradient tensor, while the vorticity field is related to the rotational part of the velocity gradient tensor. It can define the geometric information of the strain rate and vorticity by identifying the flow regions where either the strain or vorticity predominates, see (Afonso & Meneveau, 2010).

2.3 Methodology

The analytical procedures are complicated when being applied to the flow system because the analytic solution of NSE is limited for simple geometry and a low Reynolds number flow. Explaining the physics of such phenomena in turbulent flows requires both experimentation and numerical techniques. Experiments are still considered complicated to set up, and they are also expensive. In this case, digital computers and computational capacity development have motivated us to use numerical techniques to simulate turbulent flows. The main advantages of numerical simulations include that they are highly promising in generating a vast amount of data. For example, when considering a numerical simulation, we may define the value of the variables of each point in the mesh of the computational domain. At present, the three primary approaches are used for predicting turbulent flows, such as direct numerical simulation (DNS), large eddy simulation (LES), and Reynolds-Average-Navier-Stokes (RANS); for more details, see (Pope, 2001; Sagaut, 2006).

However, DNS is the obvious choice for the understanding of multiscale turbulent flow, but the grid points in DNS scales like $O\left(\mathcal{R}_e\right)^{9/4}$ (Pope, 2001) which is unfeasible with the current computing power at hand. In this context, turbulence modeling was introduced to reduce the degree of freedom of the problem, such as large eddy simulations (LES) and Reynolds-Average-Navier–Stokes (RANS). However, RANS is widely used in engineering applications where the problems are generally exhibited for $\mathcal{R}_e$ and complex geometry. Thus, LES would compromise between the cost and complexity if one is interested in studying the time-varying turbulence structures. In this approach, the simulations balance accuracy, stability, computational cost, and physical demands. A promising technique called LES has been studied in this thesis, see (Pope, 2001; Sagaut, 2006).

2.3.1 Large eddy simulation

The large eddy simulation (LES) idea was first proposed by (Smagorinsky, 1963), and later studied extensively by (Deardorff et al., 1970). In this methodology, the larger scales of turbulent motions are obtained by solving the Navier–Stokes equations. A spatial filter is applied to remove the small scales motion. The unresolved small scales almost appear homogeneous and possess a universal character, and the effect of those scales on the large scales are modeled through the subgrid-scale (SGS) model, see (Pope, 2001). It is an efficient and highly reliable method to predict the turbulent flow of properties accurately (Pope, 2001).

In this thesis, instead of using an explicit filtering operation, the second-order finite volume discretization of the flow equation is considered the numerical mesh, and it is an implicit filter. In this filter, the turbulent scales smaller than the grid mesh are known as unresolved scales, while scales greater than grid size are called the resolved scales. It is similar to the operation of a box filter when the filter width is equal to the grid spacing (Pope, 2001).

The filtered equation of continuity and Navier–Stokes equations for incompressible flow can be written as:

$$\frac{\partial \bar{u}_i}{\partial x_i} = 0, \tag{2.4}$$

$$\frac{\partial \bar{u}_i}{\partial t} + \bar{u}_j \frac{\partial \bar{u}_i}{\partial x_j} = -\frac{1}{\rho}\frac{\partial \bar{P}}{\partial x_i} + \nu \frac{\partial^2 \bar{u}_i}{\partial x_j \partial x_j} - \frac{\partial \tau_{ij}}{\partial x_j} + f_i. \tag{2.5}$$

Here $\bar{u}_i$ are the resolved scales, $\bar{P}$ is denoted the modified pressure field, ν is the kinematic viscosity, and f_i is the external force. The effect of the small scales is accounted by the subgrid-stress term τ_{ij}. So, to close the system mathematically, τ_{ij} should be parameterized.

Many studies of LES have been conducted extensively over the past several decades, see (Pope, 2001). The modeling of small scales turbulence is the main issue in the study of LES, which was initiated by the work of (Smagorinsky, 1963). There are many types of subgrid-scale (SGS) models currently using in LES method. In this thesis, the fundamental of four different dynamic eddy viscosity subgrid-scale models are considered, including dynamic model based on vortex stretching model (SGS-A) (Nicoud & Ducros, 1999), dynamic k-equation model (SGS-B) when C_k is dynamic (Kim & Menon, 1995), k-equation model (SGS-C) when C_k is fixed (Deardorff, 1972), and dynamic Lagrangian model (SGS-D) (Meneveau et al., 1996).

Most of the SGS models are based on the eddy viscosity hypothesis (Davidson, 2004). These models can compute the deviatoric part of the SGS stresses using:

$$\tau_{ij} - \frac{1}{3}\tau_{kk}\delta_{ij} = -2\nu_\tau \mathcal{S}_{ij}, \tag{2.6}$$

where δ_{ij} is the Kronecker delta, $\mathcal{S}_{ij} = \frac{1}{2}\left(\frac{\partial \bar{u}_i}{\partial x_j} + \frac{\partial \bar{u}_j}{\partial x_i}\right)$ is the resolved strain rate tensor, and ν_τ is the subgrid-scale eddy viscosity, which is approximated by the SGS models. A detailed explanation of the subgrid-scale model is discussed in the next section.

2.3.2 Models for turbulence eddy viscosity

2.3.2.1 Dynamic model based on vortex stretching model (SGS-A)

In this subgrid-scale model, the eddy viscosity is evaluated using the square of the velocity gradient tensor. The turbulent kinetic energy of the SGS-A model is given by:

$$k_{sgs} = (\Delta_{les})^2 \frac{\left(\mathcal{S}^d_{ij}\mathcal{S}^d_{ij}\right)^{3/2}}{\left(\mathcal{S}_{ij}\mathcal{S}_{ij}\right)^{5/2} + \left(\mathcal{S}^d_{ij}\mathcal{S}^d_{ij}\right)^{5/4}}, \tag{2.7}$$

where Δ_{les} is the computational grid length. If k_{sgs} is modeled by equation 2.7 then we define the scale adaptive eddy viscosity of the SGS-A model as:

$$\nu_\tau = C_s \Delta_{les} \sqrt{k_{sgs}}. \tag{2.8}$$

.

The term $\mathcal{S}^d_{ij}$ is the deviatoric symmetric part of the square of the velocity gradient tensor (Nicoud & Ducros, 1999), which is defined by:

$$\mathcal{S}^d_{ij} = \frac{1}{2}\left[\mathcal{G}_{ij} + \mathcal{G}_{ij}\right] - \frac{1}{3}\delta_{kk}\mathcal{G}_{kk}, \tag{2.9}$$

where $\mathcal{G}_{ij} = \left(\frac{\partial u_i}{\partial x_k}\right)\left(\frac{\partial u_k}{\partial x_j}\right)$. Here, the term $\mathcal{S}^d_{ij}$ is related to vortex stretching $|\mathcal{S}\boldsymbol{\omega}|$ and second invariant Q_G of the velocity gradient tensor. The term $-(1/2)\mathcal{S}^d_{ij}\mathcal{S}^d_{ij} = -(1/4)|\mathcal{S}\boldsymbol{\omega}| - (1/3)Q^2_G$ in equation 2.7 can detect the turbulent structure with the strain rate, rotation rate and vortex stretching (Nicoud & Ducros, 1999; Bhuiyan & Alam, 2020), which indicates that it adjusts the value of ν_τ dynamically on the strength of vortex stretching, as well as the relative dominance strain over rotation. The true constant C_w value is usually between 0.3 and 0.6, however, it can vary depending on the nature of turbulent flows (Nicoud & Ducros, 1999).

2.3.2.2 Dynamic k-equation model (SGS-B)

The localized dynamic kinetic energy model was proposed by (Kim & Menon, 1995), which is a similar concept to that of the dynamic Smagorinsky model by (Lilly, 1992). In this model, the model coefficients are computed by setting an additional test filter $\tilde{\Delta} = 2\Delta_{les}$ (Meneveau, 2010). The model coefficients C_k and C_e are estimated dynamically at the test filter level. The adjustable model constant C_k is determined by:

$$C_k = \frac{1}{2}\frac{\mathcal{L}_{ij}\mathcal{M}_{ij}}{\mathcal{M}_{ij}\mathcal{M}_{ij}}, \tag{2.10}$$

where, $\mathcal{L}_{ij} = \widetilde{\bar{u}_i\bar{u}_j} - \tilde{\bar{u}}_i\tilde{\bar{u}}_j$ is obtained from the filtered velocities along with the test filtering operation, and $\mathcal{M}_{ij} = -\left(2\Delta_{les}\tilde{\mathcal{S}}_{ij}\tilde{k}_{sgs}^{1/2} - \Delta_{les}\widetilde{\mathcal{S}_{ij}k_{sgs}^{1/2}}\right)$. The turbulent kinetic energy $\tilde{k}_{sgs}$ is computed at the test filtering level from the trace of $\mathcal{L}_{ij}$.

Finally, the parameter C_e is computed as:

$$C_e = \nu \left[\widetilde{\frac{\partial\bar{u}_i}{\partial x_j}\frac{\partial\bar{u}_j}{\partial x_i}} - \frac{\partial\tilde{\bar{u}}_i}{\partial x_j}\frac{\partial\tilde{\bar{u}}_j}{\partial x_i}\right] \Big/ \left[\frac{\tilde{k}_{sgs}^{1/2}}{2\Delta_{les}} - \widetilde{\frac{k_{sgs}^{1/2}}{\Delta_{les}}}\right]. \tag{2.11}$$

The adjustable value C_k and C_e are calculated dynamically in this subgrid model. It is worth mentioning that the local variation of subgrid-scale energy dissipation can be accounted for in the localized dynamic kinetic energy equation via dynamic variation of C_k, which is important in many engineering applications.

2.3.2.3 k-equation model (SGS-C)

In the TKE-based model, the turbulent kinetic energy is obtained by solving the following transport equation (Deardorff, 1972):

$$\frac{\partial k_{sgs}}{\partial t} + \bar{u}_j\frac{\partial k_{sgs}}{\partial x_j} = -\tau_{ij}\mathcal{S}_{ij} - C_e\frac{k_{sgs}^{3/2}}{\Delta_{les}} + \frac{\partial}{\partial x_j}\left(\nu_\tau\frac{\partial k_{sgs}}{\partial x_j}\right), \tag{2.12}$$

where k_{sgs} is the turbulent kinetic energy. The eddy viscosity ν_τ is estimated by using the k_{sgs} value from the equation (2.12) as:

$$\nu_\tau = C_k k_{sgs}^{1/2}\Delta_{les}, \tag{2.13}$$

where the model constant $C_k = 0.094$ is fixed, and the dissipation constant $C_e = 1.048$. In equation (2.12), the terms on right hand side describe the production of turbulence, dissipation and diffusion of turbulent kinetic energy k_{sgs}. As a result, improved versions of the k-equation model have been presented for dynamically calculating the constants based on the local turbulence. This subgrid-scale model is important for LES of atmospheric turbulence, see for the details information (Deardorff, 1972; Yoshizawa, 1986a).

2.3.2.4 Lagrangian dynamics model (SGS-D)

Meneveau et al. (Meneveau et al., 1996) proposed the LES model that averages overflow path lines instead of homogeneous directions (Meneveau, 2010). In a Lagrangian dynamic model, the model

coefficient C_s is computed along the path line by averaging inhomogeneous flow in the complex geometry, but two additional equations are required for this to be solved. In the Smagornsky model,

$$\nu_\tau = (C_s \Delta_{les})^2 |\mathcal{S}|.$$

Hence, to evaluate the model coefficient C_s in the Lagrangian dynamics model, the Lagrangian transport of two auxiliary variables $I_{lm}(\boldsymbol{x}, t)$ and $I_{mm}(\boldsymbol{x}, t)$ are determined. Thus, the value of C_s is calculated as:

$$C_s = \sqrt{\frac{I_{lm}}{I_{mm}}}. \tag{2.14}$$

For the detail information of I_{lm} and I_{mm}, see (Meneveau et al., 1996).

Models	Features(eddy-viscosity model)	References
SGS-A	vortex-stretching-based	Nicoud et al. (1999), Bhuiyan et al. (2020)
SGS-B	localized dynamic kinetic energy	Kim (1995), Chai et al. (2012)
SGS-C	TKE-based	Deardorff (1971), Yoshizawa et al. (1986)
SGS-D	Lagrangian dynamic	Meneveau et al. (1996), Bou-Zeid et al. (2005)

Table 2.1: The proposed subgrid-scale models in this thesis.

2.3.3 Statistics of the velocity and its gradient tensor

Statistics are widely used to characterize the variables of a turbulent flow field (Kundu et al., 2008) (Pope, 2001) because they are unpredictable in both time and space. In this thesis, the LES code has been developed based on a second-order accurate, linearly stable, and less-dissipative numerical scheme to minimize the effect of numerical errors. We run LES code with 32 processors and 128^3 resolution in a periodic box $[0, 2\pi]^3$ by utilizing the Graham cluster from Compute Canada. The central differencing finite volume scheme is implemented to discretize the NSE, where the trapezoidal method is employed for the time integration scheme. Finally, the pressure-implicit with the splitting of operators (PISO) algorithm is used to solve the discretized NSE (Pletcher, Tannehill, & Anderson, 2012). All of the simulations are performed in a cubical domain with a uniform grid mesh. After the simulations, the LES results of the four subgrid-scale models are gathered in a data set for statistical analysis.

2.3.3.1 First-order and higher-order moment

In this section, some useful statistical tools are defined, which are used throughout this thesis. To illustrate the *posteriori* LES field $u_i = \langle u_i \rangle + u_i^{'}$, the expected velocity field is determined from M flow of realization such that

$$\langle u_i \left(\boldsymbol{x}_k \right) \rangle = \frac{1}{M} \sum_{n=1}^{M} u_i \left(\boldsymbol{x}_k, t_n \right), \tag{2.15}$$

where $\langle . \rangle$ is denoted as the temporal average. On the other hand, the first-order moment of $u_i \left(\boldsymbol{x}_k, t_n \right)$ does not provide the information of fluctuations $u_i^{'} \left(\boldsymbol{x}_k, t_n \right)$ components.

Thus, a second order moment is the fluctuation of u_i around the mean value $\langle u_i \rangle$, which is defined by $u_i' = \langle u_i \rangle - u_i$. Now, a second order moment is written by:

$$\langle (u_i(\boldsymbol{x}_k, t^n) - \langle u_i(x_k) \rangle)^2 \rangle = \frac{1}{M} \sum_{n=1}^{M} (u_i(\boldsymbol{x}_k, t_n) - \langle u_i(\boldsymbol{x}_k) \rangle)^2, \tag{2.16}$$

where a square root of the above equation 2.16 is known as root mean square, which is obtained by (Kundu et al., 2008):

$$u_{rms} = \sqrt{\frac{1}{M} \sum_{n=1}^{M} (u_i(\boldsymbol{x}_k, t_n) - \langle u_i(\boldsymbol{x}_k) \rangle)^2}. \tag{2.17}$$

Similarly, a third-order moment is known as skewness of the velocity field, which is defined by:

$$\frac{1}{M} \sum_{n=1}^{M} (u_i(\boldsymbol{x}_k, t_n) - \langle u_i(\boldsymbol{x}_k) \rangle)^3 \rangle.$$

For the isotropic turbulence field, the first-order moment is $\langle u_i(\boldsymbol{x}_k) \rangle = 0$, while the second-order moment $\langle (u_i(\boldsymbol{x}_k, t_n) - \langle u_i(\boldsymbol{x}_k) \rangle)^2 \rangle \neq 0$.

2.3.3.2 Joint probability density function

The joint probability density function (JPDF) is a statistical property used to describe the jointly random variables on a probability space. The JPDF is an important property of random variables because they are dependent on each other in turbulent flows. For example, let X and Y are two random variables, and the JPDF of the random variables are defined by the function $J_p \left(X, Y \right)$. Assuming that the probability of the first random variable is specified in between x and $x + dx$, and the second random variable is in between y and $y + dy$. Thus, J_p is a joint probability density function of X and Y, if it satisfies these conditions: (i) $J_p \left(X, Y \right) \geq 0$, and (ii) the total probability is 1, which can be defined as $\int_{-\infty}^{\infty} \int_{-\infty}^{\infty} J_p \left(X, Y \right) dxdy = 1$. Now, the JPDF of X and Y is following this form:

$$P\{x < X < x + dx, y < Y < y + dy\} = \int_{x}^{x+dx} \int_{y}^{y+dy} J_p \left(X, Y \right) dydx.$$

The above equation is known as the joint probability density function (JPDF) (Pope, 2001) and based on the statistical theory of JPDF, as explored so far in the thesis, this thesis has shown the physical meaning of the JPDF of invariants regarding the velocity gradient tensor. The JPDF of the invariants of the velocity gradient tensor is mainly classified as the fluid flow topology, see (Dallas & Alexakis, 2013). The study of flow topology is mainly based on the analysis of the velocity gradient tensor (Martın et al., 1998), which is an essential candidate to understand the flow dynamics and turbulence generation by vortex stretching (Martín & Dopazo, 1995).

The velocity gradient tensor is $\mathcal{G}_{ij}$ (or $\mathcal{G}$) $= \dfrac{\partial \bar{u}_i}{\partial x_j}$, which is composed of a symmetric ($\mathcal{S}_{ij}$) and an anti-symmetric component (R_{ij}), where $\mathcal{S}_{ij} = \dfrac{1}{2}\left(\dfrac{\partial \bar{u}_i}{\partial x_j} + \dfrac{\partial \bar{u}_j}{\partial x_i}\right)$ is a symmetric strain rate of the tensor, and $R_{ij} = \dfrac{1}{2}\left(\dfrac{\partial \bar{u}_i}{\partial x_j} - \dfrac{\partial \bar{u}_j}{\partial x_i}\right)$ is the anti-symmetric rotation rate of tensor. Now, the characteristic equation of the velocity gradient tensor $\mathcal{G}$ is obtained by:

$$\lambda_i^3 + P_G\lambda_i^2 + Q_G\lambda_i + R_G = 0 \tag{2.18}$$

where $\lambda_i, i = 1, 2, 3$ are the eigenvalues. P_G, Q_G, and R_G are the first, second, and third invariants of the velocity gradient tensor, respectively. For incompressible flow, the first invariant is $P_G = 0$. Hence, using the strain-rate ($\mathcal{S}_{ij}$) and rotation-rate (R_{ij}), the second and third invariants of $\mathcal{G}$ can be written as:

$$\begin{cases} Q_G = -\dfrac{1}{2}\left(\mathcal{S}_{ij}\mathcal{S}_{ij} - R_{ij}R_{ij}\right) \\ R_G = -\dfrac{1}{3}\left(\mathcal{S}_{ij}\mathcal{S}_{jk}\mathcal{S}_{ki} + \dfrac{3}{4}\omega_i\omega_j\mathcal{S}_{ij}\right) \end{cases} \tag{2.19}$$

Now, the straining rate of tensor ($\mathcal{S}_{ij}$) of invariants Q_G and R_G are obtained by setting the rotation to zero in the equation 2.19, then we obtain:

$$\begin{cases} Q_S = -\dfrac{1}{2}\mathcal{S}_{ij}\mathcal{S}_{ij} \\ R_S = -\dfrac{1}{3}\mathcal{S}_{ij}\mathcal{S}_{jk}\mathcal{S}_{ki} \end{cases} \tag{2.20}$$

If the straining rate tensor is zero in Q_G of the equation 2.19, then we obtain:

$$Q_R = \frac{1}{2}R_{ij}R_{ij} \tag{2.21}$$

It is important to explore the physical meaning of the above invariants tensor. Initially, we observe the physical meaning of the second invariant (Q_G) and third invariant (R_G) of the velocity gradient tensor $\mathcal{G}$. Hence, the value $Q_G > 0$ is connected in a region where the enstrophy via the vortex-stretching is

dominant over weak total strain, while it is the reverse for $Q_G < 0$. It is also possible to identify the region by using the third invariant R_G through the Q_G value. If the invariant Q_G is much greater than zero ($Q_G \gg 0$) then the invariant $R_G \approx -\frac{1}{4}\omega_i\omega_j\mathcal{S}_{ij}$. In this case, the value of $R_G > 0$ indicates a predominant region by the vortex-stretching over the weak vortex-compression, while the reverse is true for $R_G < 0$. In contrast, if the value of Q_G is much less than zero ($Q_G \ll 0$) then the invariant $R_G \approx -\frac{1}{3}\mathcal{S}_{ij}\mathcal{S}_{jk}\mathcal{S}_{ki}$. In this instance, a region of $R_G < 0$ is associated with the enstrophy production, while $R_G > 0$ is concentrated in the viscous dissipation, see (Davidson, 2004).

In equation 2.20, the second invariant of the strain rate ($\mathcal{S}_{ij}$) is $Q_S = -\frac{1}{2}\mathcal{S}_{ij}\mathcal{S}_{ij} = -\frac{1}{2}\mathcal{S}^2$, which indicates the viscous dissipation of the turbulent kinetic energy (da Silva & Pereira, 2008). Hence, the relation between the dissipation rate (ϵ) and the second invariant strain is, $Q_S = -\frac{1}{2}\mathcal{S}_{ij}\mathcal{S}_{ij} = -\frac{\epsilon}{4\nu}$. It is noted that the invariant Q_S is a negative definite. Therefore, the large negative value of Q_S is associated with the viscous dissipation region. Moreover, the second invariant of the rotation rate in equation is 2.21 is, $Q_R = \frac{1}{2}R_{ij}R_{ij}$, which signifies the enstrophy density in a flow field. However, the second invariant rotation rate is always positive. Accordingly, the third invariant of strain rate is, $R_S = -\frac{1}{3}\mathcal{S}_{ij}\mathcal{S}_{jk}\mathcal{S}_{ki}$, where $\mathcal{S}_{ij}\mathcal{S}_{jk}\mathcal{S}_{ki}$ is called the self-amplification rate. The invariant R_S estimates the production of dissipation rate and shows the two physical meanings, see (Dallas & Alexakis, 2013).

In this thesis, in order to understand the JPDF of the velocity gradient tensor among the four subgrid-scale models, we mainly focus on the JPDF between : (i) the second invariant (Q_G) and third invariant (R_G), see equation 2.19; (ii) the straining rate of second invariant (Q_S) and straining rate of third invariant (R_S), see equation 2.20; and (iii) the second invariant strain rate ($-Q_S$) and rotation rate (Q_R), see equation 2.20 and 2.21.

2.4 Primary results

In this section, several analyses have been conducted using the subgrid-scale models before moving in Chapter 3 to finalize the results. Specifically, this discussion mainly interests to observe the performance of the vortex stretching-based subgrid-scale model SGS-A, which is based on the square of the velocity gradient tensor. Some of the most critical findings are mentioned in the following discussion.

2.4.1 The resolution effects

The resolution effects are also tested carefully. In this case, the three resolutions are tested, such as $\mathcal{N} = 64^3$, 128^3, and 256^3, where $\mathcal{N}$ is defined the number of grid points. Furthermore, the six different Reynolds numbers are examined to account for the resolution effects, such as $\mathcal{R}_e = 5 \times 10^4$, 1×10^5, 2×10^5, 3×10^5, 4×10^5, and 5×10^5. The findings suggested that the Reynolds number $\mathcal{R}_e = 5 \times 10^5$ showed a better performance at $\mathcal{N} = 128^3$ resolution in the subgrid-scale models. Hence, the Reynolds number $\mathcal{R}_e = 5 \times 10^5$ and $\mathcal{N} = 128^3$ are fixed for all the next simulations.

2.4.2 The C_w value for SGS-A model

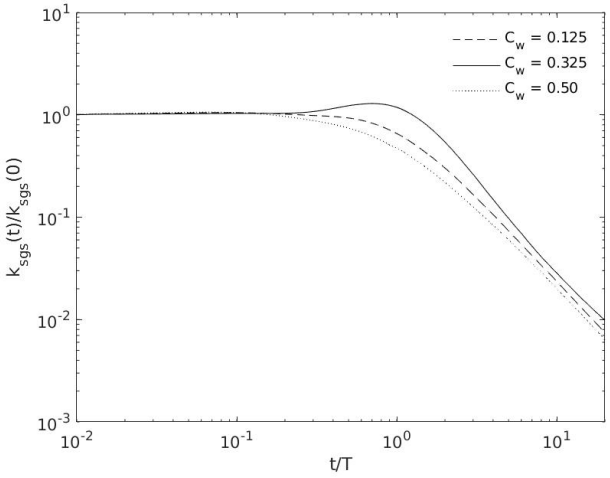

Figure 2.3: A sensitivity study of the model parameter C_w in the turbulent kinetic energy k_{sgs} for SGS-A model.

The true constant C_w in SGS-A subgrid-scale model is estimated numerically using several fields of homogeneous isotropic turbulence by the formula (Nicoud & Ducros, 1999),

$$C_w^2 = C_s^2 \frac{\langle \sqrt{2} \left(\mathcal{S}_{ij}\mathcal{S}_{ij}\right)^{3/2} \rangle}{\langle \mathcal{S}_{ij}\mathcal{S}_{ij} \frac{\left(\mathcal{S}^d_{ij}\mathcal{S}^d_{ij}\right)^{3/2}}{\left(\mathcal{S}_{ij}\mathcal{S}_{ij}\right)^{5/2} + \left(\mathcal{S}^d_{ij}\mathcal{S}^d_{ij}\right)^{5/4}} \rangle},$$

where the model parameter, $C_s = 0.18$, is the classical Smagorinsky model constant, $\mathcal{S}_{ij}$ is the strain rate, and $\mathcal{S}^d_{ij}$ is the traceless symmetric part of the square of the velocity gradient tensor. For wall-bounded flow, the C_w values are usually between 0.3 and 0.6. In this study, the sensitivity of C_w is observed for unbounded periodic flow. Thus, three different values are tested on the turbulent kinetic energy, such as $0.125, 0.325$, and 0.50. Based on the several numerical results, this thesis presents

that the model portion of turbulent kinetic energy (k_{sgs}) is dynamically adjusted as the resolved flow varies by the different value of C_w. Overall, the results of the SGS-A subgrid-scale model on the turbulent kinetic energy seem appropriate at $C_w = 0.325$, see Fig. 2.3. Hence, we assigned a C_w value to 0.325 in all simulations for this thesis.

2.4.3 A comparison between upwind and central method

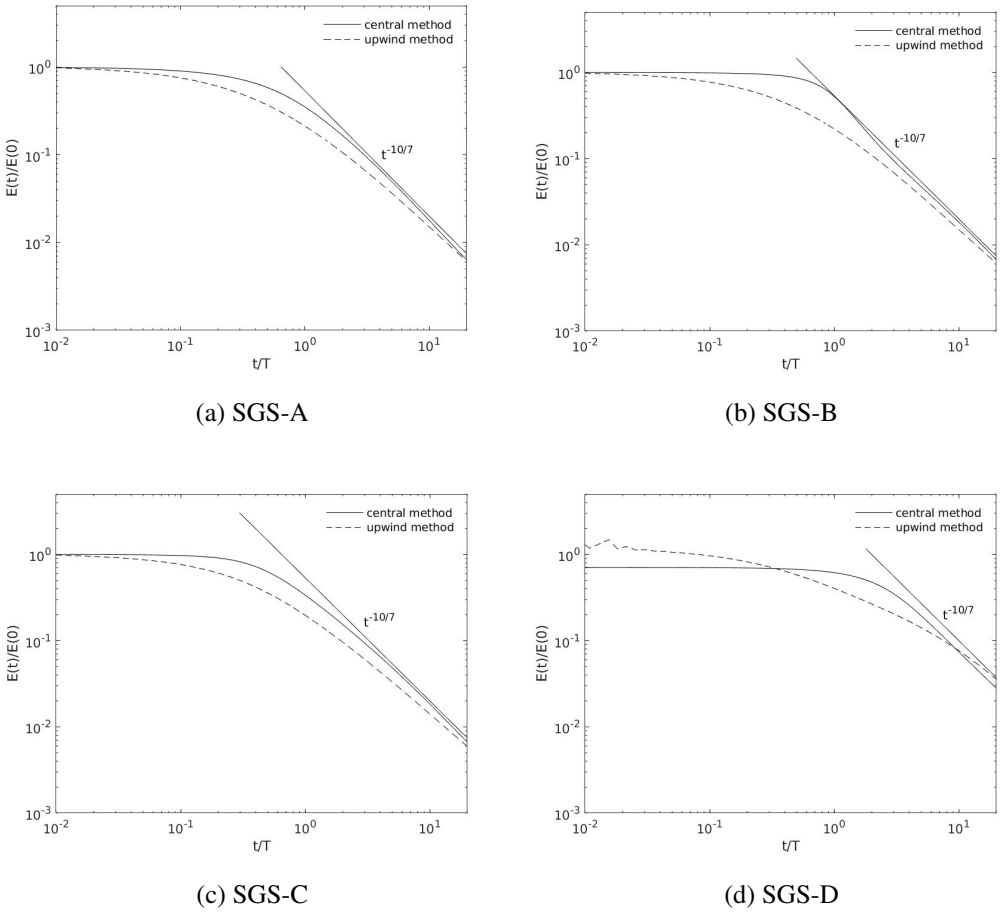

(a) SGS-A (b) SGS-B

(c) SGS-C (d) SGS-D

Figure 2.4: A comparison between the central and upwind method of four subgrid-scale models at $\mathcal{R}_e = 5 \times 10^5$ and $\mathcal{N} = 128^3$ resolution.

The most challenging aspect of the Navier–Stokes equations is to solve the non-linear advective term accurately. In finite-volume discretization, several schemes have been designed to tackle the advective term. However, it requires investigation to select a proper numerical method that accurately represents the turbulence. This thesis has tested two numerical methods in the developed LES code, namely the upwind and central methods, concerning the four subgrid-scale models. We can see from the plots 2.4 that the upwind method (Pletcher et al., 2012) is highly dissipative and diffuses all the turbulence

quickly. The upwind scheme is also extremely stable and non-oscillatory. It is very fast compared to the second-order scheme; however, it may give inaccurate results and false diffusion.

On the other hand, the central method performs better and accurately predicts the theoretical decay law in the subgrid-scale models, see Fig. 2.4 (Kolmogorov, 1941). Along with the treatment of the central method for the non-linear term, we employed a trapezoidal method for time integration which makes the 'in-house LES code' second-order accurate in space and time. Therefore, the central method is fixed for all the simulations in this thesis. The finding indicates that the SGS-A model produces sufficiently to compare with the SGS-B, SGS-C and SGS-D subgrid-scale models.

2.4.4 Skewness of the velocity gradient tensor for SGS-A model

The skewness of the velocity derivative in turbulent flows and its dependence on turbulence Reynolds number $\mathcal{R}e_\lambda$ was studied extensively in the past (Davidson, 2004). The skewness characterizes the rate of production of vorticity by vortex stretching. The non-zero value of skewness arises from a natural tendency that creates smaller scales, which is a process that is known as the energy cascade from large to small scales in physical space. Kolmogorovs theory of isotropic turbulence is based on the existence of vortices on all possible scales, see (Kolmogorov, 1962), and thus, the energy cascade can be associated with the enstrophy production by vortex stretching (Davidson, 2004). In doing so, Kolmogorov four-fifth and two-third laws are defined respectively as:

$$\langle[\Delta \boldsymbol{u}]^3\rangle = -4/5\epsilon r, \quad \eta \gg r \gg L, \tag{2.22}$$

$$\langle[\Delta \boldsymbol{u}]^2\rangle = \beta\epsilon^{3/1} r^{2/3}, \quad \eta \gg r \gg L. \tag{2.23}$$

The skewness of the velocity gradient is approximated by combining the above two laws as:

$$S_0 = -4/5\beta^{-3/2}, \quad r \longrightarrow 0. \tag{2.24}$$

where, $\beta \sim 2$ is a Kolmogorov constant. We have considered $S_0 = \lim_{r\to 0} S(r)$ by using the equation (2.24), where $S(r) = \langle[\Delta \boldsymbol{u}]^3\rangle / \langle[\Delta \boldsymbol{u}]^2\rangle^{3/2}$ is the skewness of a vector field $\boldsymbol{u}(\boldsymbol{x})$, in which the velocity increment is defined as $\Delta \boldsymbol{u} = [\boldsymbol{u}(\boldsymbol{x}+\boldsymbol{r}) - \boldsymbol{u}(\boldsymbol{x})].\boldsymbol{r}/r$. Based on the equation (2.23 - 2.24), a constant value of skewness predicted as, $S_0 = -0.3$ approximately, see (Davidson, 2004), however, the skewness value can either increase and decrease as $\mathcal{R}e_\lambda$ increases (Kolmogorov, 1962).Thus, the skewness values have been obtained from various measurements of turbulent flows which indicates

that the skewness value is more or less independent of $\mathcal{R}e$, and lies in the range -0.5 to -0.4. After some algebraic manipulation, see (Davidson, 2004), we obtain the skewness as:

$$S_0 = -\frac{6\sqrt{15}\langle\omega_i\omega_j\mathcal{S}_{ij}\rangle}{7|\langle\omega\rangle|^{3/2}}. \tag{2.25}$$

Fig. 2.5 is estimated by using formula (2.25) of SGS-A subgrid-scale model for six values of Taylor Reynolds numbers $\mathcal{R}e_\lambda$. It shows that the average values of them are lying in the given literature, see (Davidson, 2004; Kolmogorov, 1962).

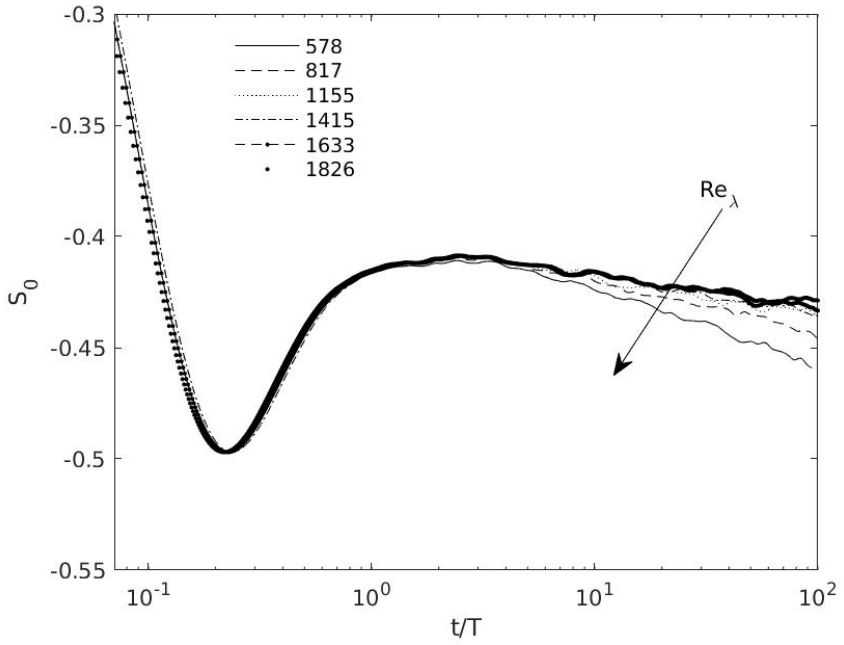

Figure 2.5: The time evolution of the skewness of the velocity gradient tensor for SGS-A model.

2.4.5 Comparison between JPDF of second and third invariants

The JPDF between the second and third invariant of the velocity gradient tensor at $t/T = 1$, and $t/T = 10$ are examined whether the statistics are stationary or not. Fig. 2.6 shows that the JPDF at $t/T = 1$ and $t/T = 10$ indicate that the stationary statistics, where the turbulence is decaying in the subgrid-scale models. As we can see in the plots 2.6 that the subgrid-scale models are more correlated due to less dispersion at $t/T = 1$, while the subgrid-scale models are less correlated due to more dispersion at $t/T = 10$, see (Dallas & Alexakis, 2013; da Silva & Pereira, 2008). However, the teardrop shapes are appeared at both eddy-turn over time among the subgrid-scale models, which indicates the similar accuracy in the subgrid-scale models.

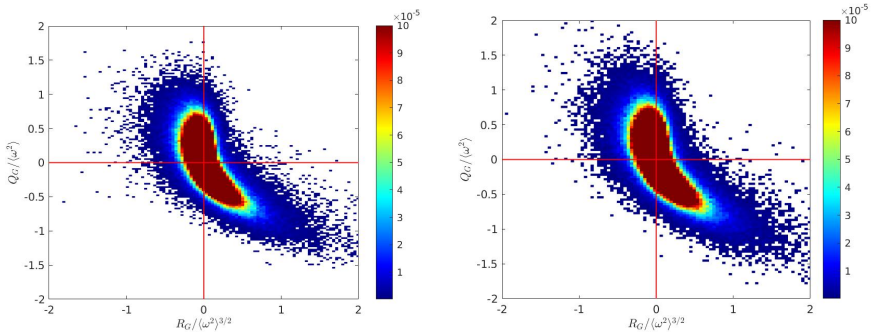

(a) SGS-A, t/T = 1 (b) SGS-A, t/T = 10

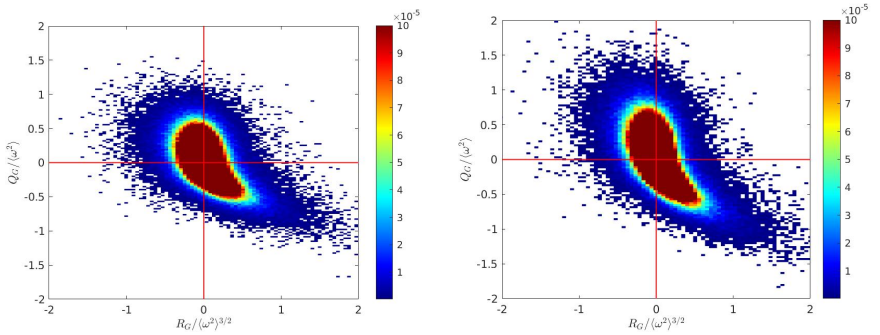

(c) SGS-B, t/T = 1 (d) SGS-B, t/T = 10

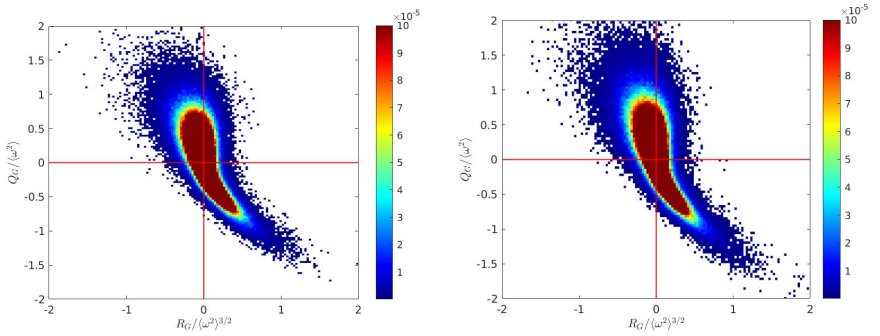

(e) SGS-C, t/T = 1 (f) SGS-C, t/T = 10

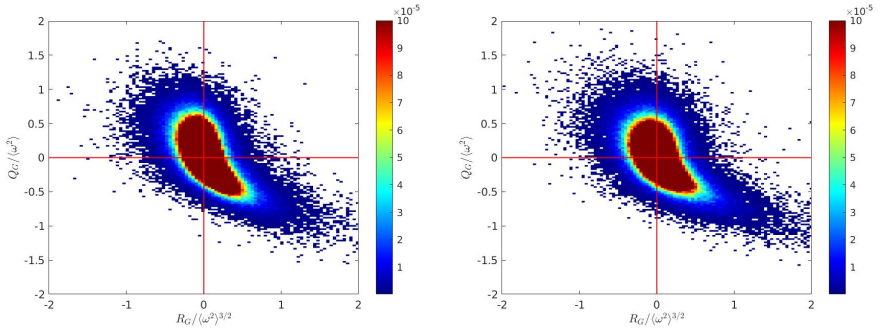

(g) SGS-D, t/T = 1 (h) SGS-D, t/T = 10

Figure 2.6: The JPDF of Q_G and R_G of the subgrid-scale models at $t/T = 1$, and $t/T = 10$.

2.4.6 Comparison between JPDF of self-amplification and enstrophy rate

The joint probability density function between the strain self-amplification $(\mathcal{S}_{ij}\mathcal{S}_{jk}\mathcal{S}_{ki})$ and the enstrophy production rate $(\omega_i\omega_j\mathcal{S}_{ij})$ is observed among the subgrid-scale models. The findings in the Fig. 2.7 of the subgrid-scale models demonstrate how enstrophy production prevents strain generation and vice versa (Buxton et al., 2017). Because the term $\omega_i\omega_j\mathcal{S}_{ij}$ is the enstrophy production rate due to vortex-stretching, and $\mathcal{S}_{ij}\mathcal{S}_{jk}\mathcal{S}_{ki}$ is the sink of the dissipation rate, which are constituted as the third invariant R_G of the velocity gradient tensor. Fig. 2.7 shows similar accuracy among the subgrid-scale models except for the SGS-C model, where the SGS-C model shows more dissipative than other subgrid-scale models.

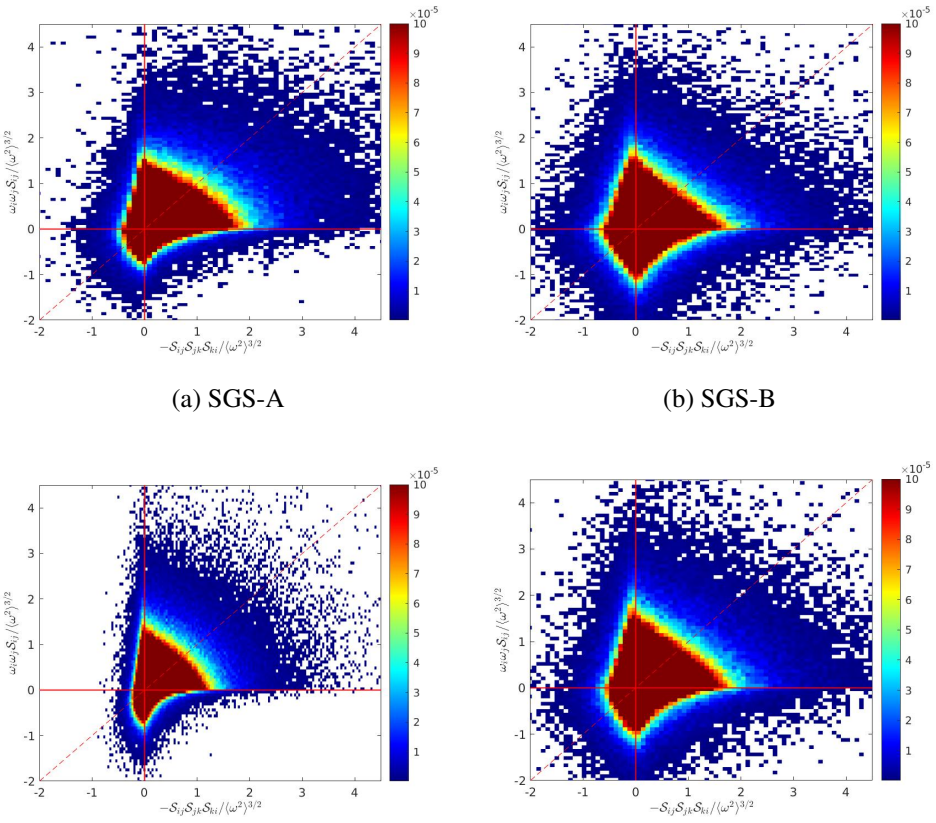

(a) SGS-A (b) SGS-B

(c) SGS-C (d) SGS-D

Figure 2.7: The JPDF of $-\mathcal{S}_{ij}\mathcal{S}_{jk}\mathcal{S}_{ki}$ and $\omega_i\omega_j\mathcal{S}_{ij}$ of the subgrid-scale models at $t/T = 1$.

2.4.7 The vortex identifications

The coherent structures of the subgrid-scale models are observed. A comparison of the simulated vortical structures is presented by the Q-criterion in Fig. 2.8. Here, $Q_G = -\frac{1}{2}(\mathcal{S}_{ij}\mathcal{S}_{ij} - R_{ij}R_{ij})$ is a second invariant of the velocity gradient tensor $\mathcal{G}$, which defines a vortex core as a connected fluid

region of $Q_G > 0$ (Lesieur et al., 2005). A fluid region of $Q_G > 0$ implies that $R_{ij}R_{ij} > \mathcal{S}_{ij}\mathcal{S}_{ij}$, and indicates that the rate of rotation dominates over the strain rate. Fig. 2.8 shows the iso-surfaces of $Q_G > 0$ of four subgrid models color by vorticity, where the red and blue colors indicate the positive and negative value of the vorticity.

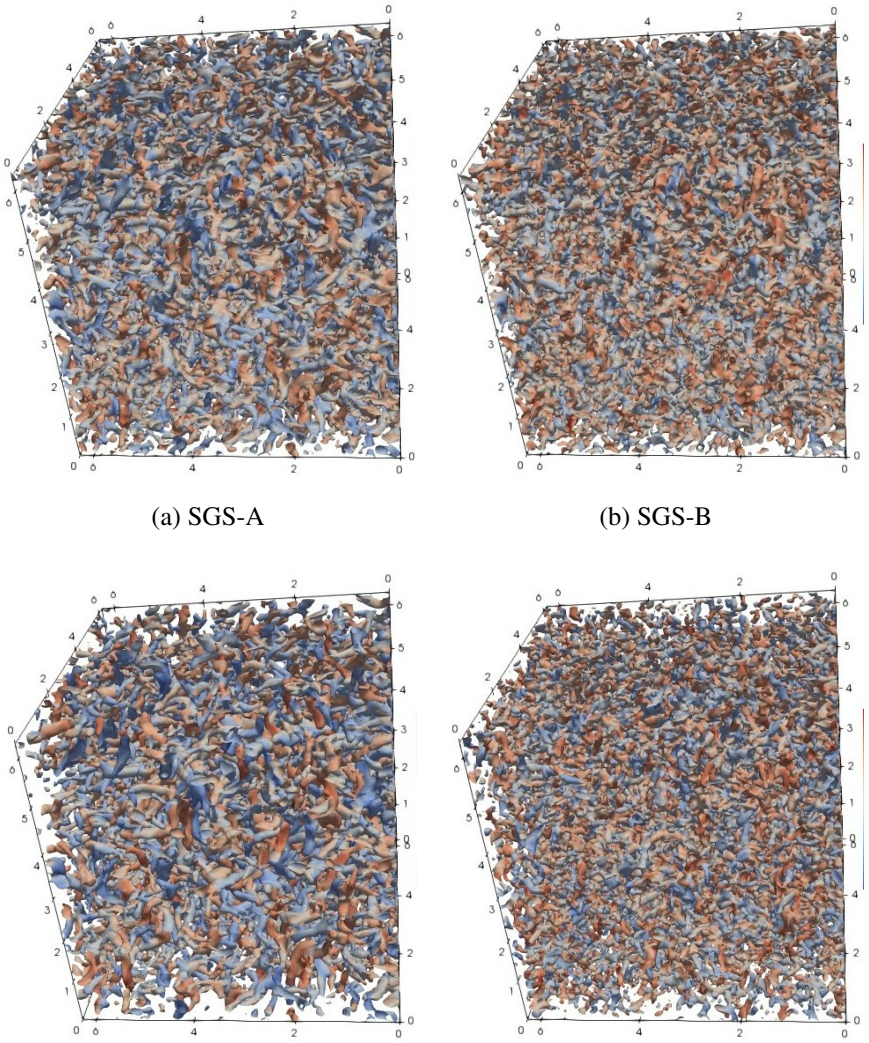

(a) SGS-A (b) SGS-B

(c) SGS-C (d) SGS-D

Figure 2.8: A visualization of contour iso-surfaces by the second invariant Q_G of the SGS models.

Fig. 2.8 shows a level of tube-like coherent structures are randomly oriented in the LES data for SGS-A, SGS-B, SGS-C and SGS-D models by setting $Q = 1$. The displayed coherent structures, of course, are dependent on the Q threshold value. However, if we change the value of Q, we can see that the LES data contains essentially the same tube-like structures with slightly different displayed representations. The current study demonstrates that coherent tube-like structures can be found in LES data and that these structures are highly unique and different, as seen in Fig. 2.8. The appearance

of the vortical structures using SGS-A is noticeably higher than that of SGS-B, SGS-C, and SGS-D, which again suggests that the accuracy of LES calculation. These observations prove that the present 'in-house LES' code can produce resolved scale turbulence by using SGS-A, SGS-B, SGS-C, and SGS-D models.

2.4.8 Force turbulence for SGS-A model

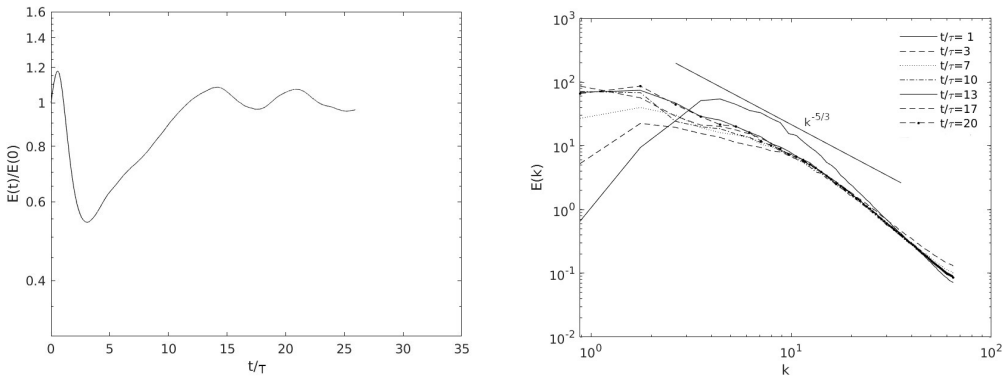

(a) (b)

Figure 2.9: (a) The time evolution of resolved kinetic energy and (b) the energy spectrum for forcing turbulence.

The forcing turbulence for SGS-A subgrid-scale model is analyzed to observe the performance of the model. A forcing term (f_i) is added in the filtered NSE 3.2 to understand the forcing turbulence case. Because of the dissipative impact of viscosity, homogeneous isotropic turbulence will decay in the absence of any production mechanism. Thus, If statistical stationery is to be maintained, body forces might be introduced to the momentum equation of the flow in terms of forcing scheme. The resolved kinetic energy plot 2.9(a) shows a trend in the energy profile, where it illustrates how the energy-containing large eddies transferred the energy to small eddies for the forcing turbulence case. As can be seen in the plot 2.9(a), the trend of energy is recovered in the stationary state from $t/T = 12$ eddy turn-over time.

The energy spectrum plots for several eddy turn-over times are presented in 2.9(b). It demonstrates how turbulent kinetic energy is distributed among the different sizes of eddies for the forcing case. The force is linearly shared among the wavenumbers, where the energy spectrums show almost identical decay after $t/T = 12$. The decay of energy is closely matched with the power law of $k^{-5/3}$ by definig

the inertial subrange.

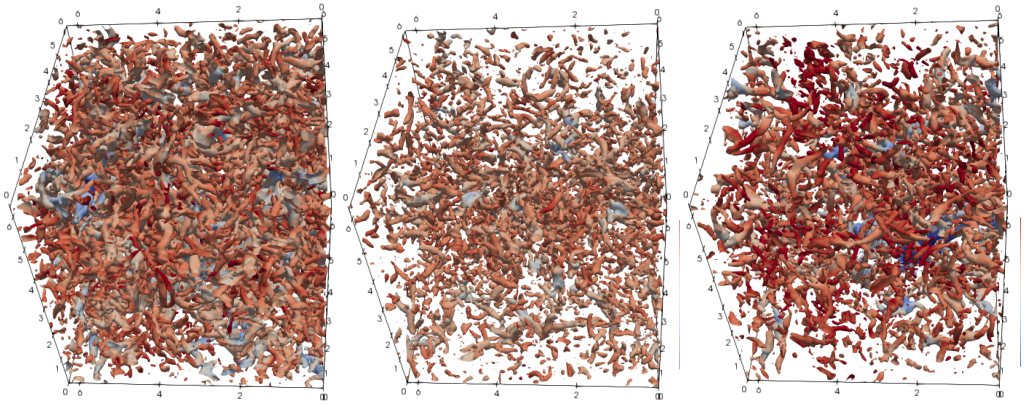

(a) t/T =1 (b) t/T =3 (c) t/T =14

Figure 2.10: The contour iso-surfaces by the second invariant Q_G of the SGS-A model.

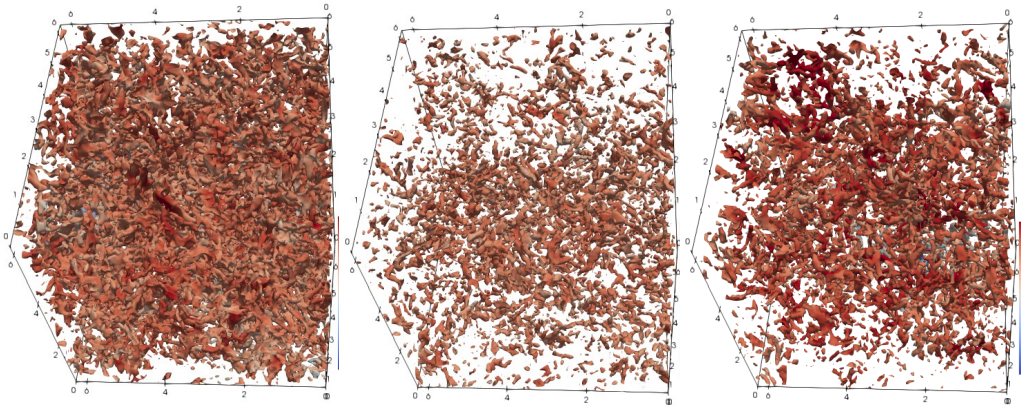

(a) t/T =1 (b) t/T =3 (c) t/T =14

Figure 2.11: The contour iso-surfaces by the negative eigenvalue λ_2-criterion of the SGS-A model.

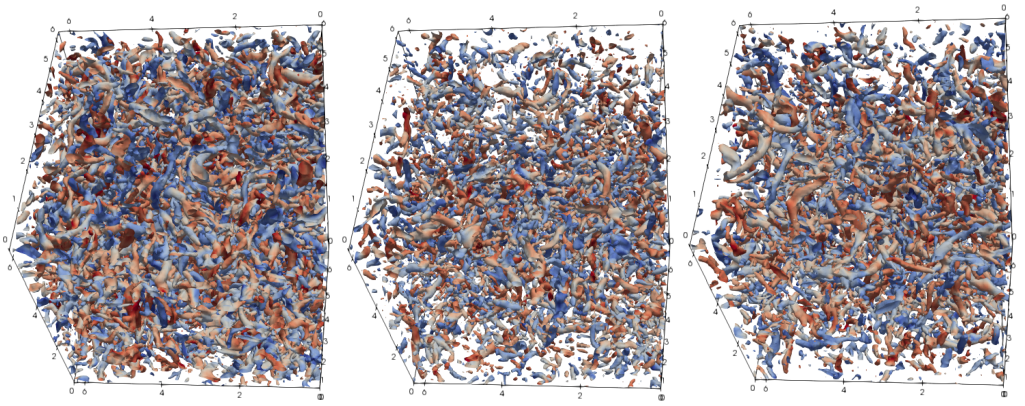

(a) t/T =1 (b) t/T =3 (c) t/T =14

Figure 2.12: The contour iso-surfaces by the vorticity of the SGS-A model.

The Kolmogorov $-5/3$ law states that in some inertial subrange $[k_1, k_2]$, the kinetic energy $E(k)$

density behaves like $C_k\epsilon^{2/3}k^{-5/3}$, where k_1 and k_2 are the wavenumbers of k. These findings conclude that the SGS-A model has shown a good agreement with the literature (Rosales & Meneveau, 2005; Lundgren, 2003). The coherent structures of the subgrid-scale model SGS-A are studied through the three popular techniques (Lesieur et al., 2005), such as Q-criterion, the negative eigenvalue λ_2-criterion, and vorticity for force turbulence. The figures 2.10, 2.11, 2.12 tell us that when the energy is higher at $t/T = 1$, it can capture sufficient tube-like structures. When the energy is lower at $t/T = 3$, the tube-like structures are showing lower. Finally, when the energy recovery the stationary state at $t/T = 14$, it is showing almost similar tube-like structures like $t/T = 1$, see Fig. 2.9(a) and Fig. 2.10, 2.11, 2.12.

2.5 Summary of accomplishments

Chapter 2 mainly focuses on the theoretical discussion to represent a vortex stretching-based subgrid-scale model (SGS-A), which is based on the square of the velocity gradient tensor. The results in this chapter indicate that SGS-A subgrid-scale model is produced accurately by the 'in-house LES code.' The results also suggest that the SGS-A model can be studied to understand the subgrid-scale dissipation of small scale motions and predict the satisfactory turbulence statistics of the velocity gradient tensor without any burden of expensive computational cost. Hence, the preliminary results of Chapter 2 are the inspiration to design a study of vortex stretching-based subgrid-scale model and to write an article along with the intent to publish it. Based on Chapter 2, considering the statistics of the velocity gradient tensor, this thesis focuses on the rate of subgrid-scale dissipation, which is presented in Chapter 3.

Chapter 3

Statistical analysis of the role of vortex stretching in LES

Citation:

Mohammed Khalid Hossen, Jahrul Alam and Asokan Variyath (2021), Statistical analysis of the role of vortex stretching in large eddy simulation, Proceedings of the 29th Annual Conference of the Computational Fluid Dynamics Society of Canada, CFDSC2021.

3.1 Abstract

The production and dissipation of vorticity in a turbulent flow is a complex process. Vortex stretching is a primary mechanical process leading to high rate of dissipation in turbulent motions. In this paper, we review some recent advances in the vorticity-based dynamic subgrid model for large eddy simulation. Considering the square of the velocity gradient tensor to detect strain, rotation, and vortex stretching, we focus on modeling subgrid-scale energy dissipation. *A posteriori* analysis of the statistics of velocity and its gradient tensor is considered. Comparing the results of 4 dynamic subgrid-scale models, it is observed that the vortex-stretching-based model accounts for relatively more subgrid-scale energy. The joint probability distribution of the second and the third invariant of the resolved velocity gradient tensor indicate that both are highly correlated regardless of whether the diffusion of vorticity or that of momentum is regarded in treating the dissipation of turbulent motion. However, the fraction of turbulence kinetic energy (TKE) appears to be relatively high in simulations based on the "vorticity transport" theory, which suggests the active role of vortex stretching in

turbulence energy cascade.

3.2 Introduction

Turbulence is a high-dimensional dynamical system. In large eddy simulation (LES) of turbulent flows, it is a challenging endeavor to capture a majority of energy containing eddies due to limited spatial and temporal resolution. In this research, we are interested in the potential role of vortex stretching so that one may statistically learn about the rate of subgrid-scale energy dissipation. An alternative approach, commonly used in the industry, is to solve additional transport equations in order to close the filtered Navier-Stokes system. In this article, we study how LES may learn the rate of subgrid-scale dissipation using statistically representative coherent flow structures.

The use of instantaneous vortices in computations of fluid flows has proven to be one of the simplest ways of understanding and computing a wide variety of turbulent flows. The pioneering work of Taylor in 1932 (Taylor, 1932) explains how vortex stretching drives the energy from the largest to the smallest scales of turbulent motion. For example, the lift – generated by a wing – and other fluid-solid interactions come from vortex motion. Rotational flow in the atmosphere and oceans can be described extremely well by collections of vortices. Nevertheless, no consensus exists on how to engage vortex stretching in subgrid parameterization schemes for LES. Sagaut & Cambon (Sagaut & Cambon, 2008) provides mathematical details of vortex stretching and energy dissipation. In (Carbone & Bragg, 2020), a statistical methodology is considered to explain vortex stretching and strain self-amplification in homogeneous isotropic turbulence. Past studies, such as (Taylor, 1932, 1938; Onsager, 1949; Leonard & Peters, 2011), indicate that the role of vortex stretching is important in describing the dynamics of turbulence (Bernard et al., 1992; Bradshaw, 1997; Davidson, 2004; Kundu et al., 2008; Tennekes & Lumley, 2018).

Hirota et al. (Hirota et al., 2017) investigated the effects of vortex stretching in homogeneous isotropic turbulence using a direct numerical simulation (DNS) approach. Shetty et al. (Shetty & Frankel, 2013) reviewed the performance of the stretched-vortex subgrid model for wall-bounded turbulence. Nicoud & Ducros (Nicoud & Ducros, 1999) proposed the wall-adapting local eddy viscosity (WALE) model for wall-bounded turbulence. Recent studies of the WALE model indicate that vortex stretching can be combined with the statistics of the velocity gradient tensor in order to detect both the statistically representative coherent structures and the instantaneous coherent vor-

tices (J. M. Alam & Fitzpatrick, 2018; Bhuiyan & Alam, 2020; Trias et al., 2015). The invariants of the velocity gradient tensor are particularly important in turbulent flows, which provide the necessary small scale information useful to close the filtered Navier-Stokes system (Martın et al., 1998; Nicoud & Ducros, 1999; da Silva & Pereira, 2008; Davidson, 2004; Lund & Novikov, 1992).

In the present analysis, we compare *a posteriori* statistics of the results of LES, using 4 subgrid models in order to assess how a subgrid model learns about subgrid-scale dissipation using the statistics of the velocity gradient tensor (Nicoud & Ducros, 1999; Trias et al., 2015). In the absence of high-resolution measurements of actual turbulent flows, such a comparison of simulated turbulence help to understand how subgrid models may be developed using statistical learning of coherent flow structures.

This article is organized as follows. In section 3.3, details of the LES method and subgrid models are discussed. The role of coherent vortices in the dissipation of subgrid-scale turbulence is discussed in section 3.4. Finally, section 3.5 provides some concluding remarks on future research directions.

3.3 Data collection and analysis

3.3.1 Filtered Navier-Stokes equation

Applying a filtering operation onto the velocity field such that $u_i = \bar{u}_i + u_i^{'}$, we get the filtered Navier-Stokes equations, where

$$\frac{\partial \bar{u}_i}{\partial x_i} = 0, \tag{3.1}$$

$$\frac{\partial \bar{u}_i}{\partial t} + \bar{u}_j \frac{\partial \bar{u}_i}{\partial x_j} = -\frac{1}{\rho}\frac{\partial \bar{P}}{\partial x_i} + \nu \frac{\partial^2 \bar{u}_i}{\partial x_i^2} - \frac{\partial \tau_{ij}}{\partial x_j} \tag{3.2}$$

Here $\bar{P}$, ρ , and ν are the modified pressure, density, and kinematic viscosity, respectively. The subfilter scale stress tensor τ_{ij} arises due to filtering the non-linear term, and such stresses

$$\tau_{ij} = \overline{u_i u_i} - \bar{u}_i \bar{u}_j, \tag{3.3}$$

represent the interactions between the motion at subfilter scales and those at resolved scales (Pope, 2001). Eq (3.2) can be closed through the eddy-viscosity model

$$\tau_{ij} - \frac{1}{3}\tau_{kk}\delta_{ij} = -2\nu_\tau \mathcal{S}_{ij} \tag{3.4}$$

which relates the unknown quantity τ_{ij} to the strain rate $\mathcal{S}_{ij} = \frac{1}{2}\left(\frac{\partial \bar{u}_i}{\partial x_j} + \frac{\partial \bar{u}_j}{\partial x_i}\right)$ of the resolved turbulence, where δ_{ij} denotes the Kronecker delta, and ν_τ is the subgrid-scale viscosity. From Eq (3.2) and Eq (3.4), we see that the eddy viscosity model is purely dissipative. This model is not fully appropriate because energy can locally flow from small to large scales in 3D turbulence, which is known as energy backscatter. The stochastic parameterization approach is one way of addressing this problem, a discussion of which is outside the scope of the present study. The idea of dynamic subgrid model is to partially address the challenge of energy backscatter.

The mathematical details of all of the 4 subgrid modeling techniques are limited by the number of pages. Briefly, we want to compute $\nu_\tau(\boldsymbol{x}, t)$ dynamically so that Eq (3.4) adapts to the local variation of subgrid-scale energy dissipation. In the rest of this article, SGS-D refers to 'Lagrangian dynamic' subgrid model in which ν_τ is calculated using the Lagrangian history of turbulence (Meneveau et al., 1996). SGS-C refers to TKE-based Deardorff model (Deardorff, 1972) commonly used in the study of atmospheric turbulence . SGS-B is the 'localized dynamic kinetic energy equation' model (Yoshizawa, 1986b), which is based on the assumption that the turbulence viscosity no longer depends upon the resolved rate-of-strain, as in the classical Smagorinsky approach, but on the subgrid-scale turbulence kinetic energy (TKE). As discussed below, SGS-A is based upon the assumption that a vortex tube can be stretched to transfer energy toward smaller scales, and the vortex stretching vector can be used for the dynamic computation of $\nu_\tau(\boldsymbol{x}, t)$ (Nicoud & Ducros, 1999).

3.3.2 Vortex stretching and subgrid-scale model

Following the classical Smagorinsky model (Smagorinsky, 1963), we have

$$\nu_\tau = (C_s \Delta_{les})^2 |\mathcal{S}|. \tag{3.5}$$

In Eq (3.5), we see that only the symmetric part $\mathcal{S}$ of the velocity gradient tensor is considered. In practice, $|\mathcal{S}|$ may be large even when turbulence production is small, and hence, an extremely small filter width Δ_{les} (or grid spacing) is needed to properly scale the eddy viscosity. We can improve the eddy viscosity model, Eq (3.5), by considering invariants of the velocity gradient tensor $\mathcal{G}_{ij} = \partial \bar{u}_i / \partial x_j$.

The first invariant, $\mathcal{G}_{ii}$, vanishes due to Eq (3.1). The second invariant, $Q_G = (1/2)\left(\mathcal{R}_{ij}\mathcal{R}_{ij} - \mathcal{S}_{ij}\mathcal{S}_{ij}\right)$, identifies coherent vortices using the relative order of magnitude between the symmetric ($\mathcal{S}_{ij}$) and the

skew-symmetric ($\mathcal{R}_{ij}$) parts of the velocity gradient tensor. The vortex stretching vector $\mathcal{S}_{ij}\omega_j$, where $\omega_j = \epsilon_{ijk}\mathcal{R}_{ij}$ is the vorticity, can be related to Q_G. Consider the symmetric part of the square of the velocity gradient tensor, and the corresponding deviatoric part,

$$\mathcal{S}^d_{ij} = \frac{1}{2}\left[\left(\frac{\partial \bar{u}_i}{\partial x_j}\right)^2 + \left(\frac{\partial \bar{u}_j}{\partial x_i}\right)^2\right] - \frac{1}{3}\delta_{ij}\left(\frac{\partial \bar{u}_k}{\partial x_k}\right)^2. \tag{3.6}$$

In $\mathcal{S}^d_{ij}$ both strain rate ($\mathcal{S}_{ij}$) and the rotation rate ($\mathcal{R}_{ij}$) are considered. However, directly replacing $\mathcal{S}$ with $\mathcal{S}^d$ in Eq (3.5) is dimensionally incorrect. It can be shown that $\mathcal{S}^d_{ij}\mathcal{S}^d_{ij} = (1/2)|\mathcal{S}\boldsymbol{\omega}| + (2/3)Q^2_G$. Using $\mathcal{S}^d_{ij}\mathcal{S}^d_{ij}$, the eddy viscosity is defined by (see (Nicoud & Ducros, 1999)),

$$\nu_\tau = (C_w\Delta_{les})^2\frac{(\mathcal{S}^d_{ij}\mathcal{S}^d_{ij})^{3/2}}{(\mathcal{S}_{ij}\mathcal{S}_{ij})^{5/2} + (\mathcal{S}^d_{ij}\mathcal{S}^d_{ij})^{5/4}}. \tag{3.7}$$

It can be seen that Eq (3.7) adjusts the value of ν_τ dynamically based on the strength of vortex stretching, as well as the relative dominance of strain $\mathcal{S}$ over rotation $\mathcal{R}$. The parameter C_w can be prescribed according to a desired average rate of dissipation. It is worth mentioning that the eddy viscosity in SGS-A, Eq (3.7), learns about subgrid-scale energy production rate from the statistics of velocity gradient tensor.

3.3.3 Statistics of velocity gradient tensor

We now discuss a statistical methodology for the evaluation of various subgrid-scale models in LES. For *a posteriori* analysis of turbulence statistics, consider M realizations of a random vector field $\{u_i(\boldsymbol{x}_k, t_n)\}$, $i = 1, 2, 3$, $k = 1, \ldots, \mathcal{N}$, and $n = 1, \ldots, M$, which can be arranged as a matrix $\mathcal{X} = [\mathcal{U}^1|\mathcal{U}^2|\cdots|\mathcal{U}^M]$ of size $3\mathcal{N}\times M$. The variability in $\mathcal{X}$ is studied by decomposing $u_i = \langle u_i\rangle + u_i'$. For instance, the temporal average is

$$\langle u_i(\boldsymbol{x}_k)\rangle = \frac{1}{M}\sum_{n=1}^{M} u_i(\boldsymbol{x}_k, t_n).$$

Higher order moments are defined by

$$\langle (u_i(\boldsymbol{x}_k, t_n) - \langle u_i(\boldsymbol{x}_k)\rangle)^m\rangle = \frac{1}{M}\sum_{n=1}^{M}(u_i(\boldsymbol{x}_k, t_n) - \langle u_i(\boldsymbol{x}_k)\rangle)^m.$$

The second moment $u^2_{\text{rms}} = \langle u_i(\boldsymbol{x}_k, t_n) - \langle u_i(\boldsymbol{x}_k)\rangle)^2\rangle$ and the third moment $S_0 = \langle u_i(\boldsymbol{x}_k, t_n) - \langle u_i(\boldsymbol{x}_k)\rangle)^3\rangle$ are variance and skewness, respectively. In statistics, skewness is a measure of the asymmetry of the probability distribution of a real-valued random variable about its mean. A negative

skewness indicates that the tail of a distribution is on the left side. According to Taylor's hypothesis of frozen turbulence the skewness of temporal variability is equivalent to that of the spatial variability in $\mathcal{X}$. A value of $S_0 \approx -0.4 + \pm 0.1$ is usually observed in experiment and direct numerical simulations, which indicates a measure of modeling accuracy in LES.

In LES, the number of grid points $\mathcal{N}$ is usually a few million and the number of time steps M is a few thousands. Statistical analysis of such a large volume of data using R or Python packages maybe less computationally efficient compared to C++ programming language. In C++, Boost Math Toolkit and Xtensor are two important libraries useful in statistical analysis. In the present study, we have utilized such tools along with the computational fluid dynamics code, OpenFOAM.

3.4 Results and Discussions

For the present study, we utilized the Graham cluster of Compute Canada to run the LES codes. All reported results corresponds to a Reynolds number at $\mathcal{R}e = 5 \times 10^5$ and 128^3 grid points in a periodic box $[0, 2\pi]^3$, unless it is mentioned otherwise. Table 3.1 reports the average values of Taylor microscale $\lambda = \sqrt{15\nu u_{rms}^2/\langle\epsilon\rangle}$, Kolmogorov's microscale $\eta = (\nu^3/\langle\epsilon\rangle)^{1/4}$, Taylor Reynolds number $\mathcal{R}e_\lambda = u_{rms}\lambda/\nu$, and the viscous dissipation rate $\langle\epsilon\rangle$. The rate of viscous dissipation is found largest in the localized dynamic kinetic energy model (SGS-B) and the smallest in the Lagrangian dynamic model (SGS-D).

Models	λ	η	$\mathcal{R}e_\lambda$	$\langle\epsilon\rangle$
SGS-A	0.27	5.971e-04	21800	0.0629
SGS-B	0.26	5.049e-04	20000	0.1231
SGS-C	0.30	5.871e-04	23000	0.0673
SGS-D	0.25	7.330e-04	12000	0.0277

Table 3.1: Values of λ, η, $\mathcal{R}e_\lambda$, and $\langle\epsilon\rangle$ estimated from the collected data $\mathcal{X}$ corresponding to 4 subgrid models.

3.4.1 Skewness and velocity gradient tensor

The skewness S_0 is related to the spatial variability in the turbulence data $\mathcal{X}$, and thus to the rate of energy transfer. Considering the spatial average with respect to rows in $\mathcal{X}$, it can be shown for isotropic turbulence that (Davidson, 2004)

$$S_0 = -\frac{6\sqrt{15}\langle\omega_i\omega_j\mathcal{S}_{ij}\rangle}{7\langle\omega_i\omega_i\rangle^{3/2}}.$$

A negative value of skewness of the data in each column of $\mathcal{X}$ tells us that the net effect of the strain field is to create enstrophy, that is, average enstrophy production by vortex stretching, $\langle\omega_i\omega_j\mathcal{S}_{ij}\rangle$, is positive. Figure 3.1 shows the temporal evolution of S_0 corresponding to columns of $\mathcal{X}$. For SGS-A and SGS-C, the skewness keeps an equilibrium value of nearly -0.4 for $t/T > 0.1$. A value of $S_0 \approx -0.4 \pm 0.1$ is usually observed in laboratory measurements of isotropic turbulence. The discrepency in S_0 depicted in Figure 3.1 may be attributed to the choice of parameters, such as C_s and Δ_{les}, or to the choice of an appropriate tensor in the definition of ν_τ (Trias et al., 2015).

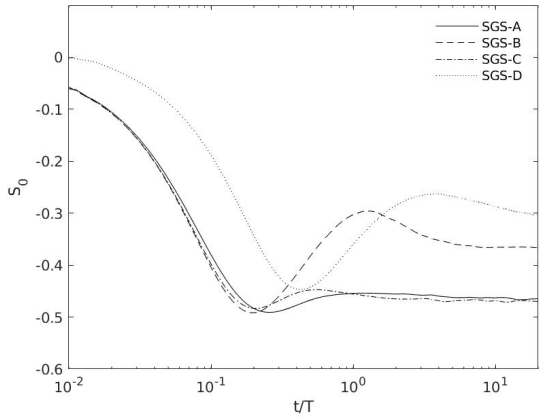

Figure 3.1: Temporal evolution of the skewness S_0 of velocity gradients for four subgrid models.

The LES results tell us two important messages. First, an approximate balance between the production of enstrophy and viscous dissipation can be achieved through the singular values of the velocity gradient tensor. In other words, a subgrid model can be dynamically learned through the velocity gradient tensor. Second, the net effect of vortex stretching is to transfer the kinetic energy that is associated with the production of enstrophy, indicating a natural tendency that creates smaller scales. In other words, the existence of vortices on all possible scales, see (Kolmogorov, 1962), indicates that the enstrophy production by vortex stretching corresponds to the energy transfer from large to small scales (Davidson, 2004).

3.4.2 Second moment of the velocity field

In homogeneous isotropic turbulence, the second moment of the spatial fluctuations of the velocity field $\mathcal{X}$ is the resolved turbulence kinetic energy, $E(t) = (1/2)\langle \boldsymbol{u} \cdot \boldsymbol{u} \rangle$ (Pope, 2001). It is widely accepted that the temporal evolution of kinetic energy in homogeneous isotropic turbulence follows Kolmogorov's decay law $E(t) \sim (t - t_0)^{-10/7}$ (Davidson, 2004).

Figure 3.2a indicates that the decay of the resolved TKE at $\mathcal{R}e = 5 \times 10^5$ is not sensitive to the choice of subgrid models considered, except that the virtual origin t_0 for the decay of energy has been shifted for the dynamic Lagrangian model (SGS-D). The velocity field $\mathcal{X}$, obtained from LES, consists of filtered and subfilter scale motions, where the trace of the residual stress $\tau_{ii} = \mathrm{Tr}(\overline{\mathrm{u_i u_j}} - \bar{\mathrm{u}}_\mathrm{i}\bar{\mathrm{u}}_\mathrm{j})$ represents the turbulence kinetic energy k_{sgs} of flow structures smaller than the cutoff scale Δ. *A posteriori* reconstruction of k_{sgs} from $\mathcal{X}$ help understand the fraction of subfilter scale TKE captured by an individual model. Figure 3.2b compares $k_{\mathrm{sgs}} = (1/2)\tau_{ii}$ among 4 subgrid models. Usually, a measure of filtering is given by the ratio of k_{sgs} to E. As the filtering was applied implicitly, *a posteriori* calculation of such a ratio requires an additional step of constructing the filtering operations. In the present study, relatively large values in the time series of k_{sgs} for SGS-A are due to the consideration of vortex stretching. Based on the calculation of skewness S_0 and the rate of energy decay $t^{-10/7}$, it can be seen that the accuracy of LES is relatively insensitive to the choice of a subgrid model. However, with respect to the ability of a subgrid model representing a relatively large fraction of the unknown residual energy, it can be seen that consideration of vortex stretching is important.

Figure 3.2(c) compares the energy spectrum $E(k)$ at $t/T = 3$ among 4 cases. The distribution of energy in Fourier space, $E(k)$, is expected to follow Kolmogorov's power law $k^{-5/3}$. In both SGS-B and SGS-D, the amount of subgrid-scale dissipation is determined through an *ad hoc* test-filtering approach without considering the coherent vortices. The dynamic process inherent in these two models aims to diffuse the momentum carried by the coherent vortices. From Table 3.1, we see that $\lambda \sim 315\eta$ and $\Delta_{les} \sim 115\eta$. The eddies of size $\mathcal{O}(\lambda)$ are only marginally resolved. Direct numerical simulations of isotropic turbulence in a periodic cube shows that the peak vorticity is largely organized into a sparse network of vortex tubes having diameters between η and λ (Davidson, 2004). In other words, variations in $E(k)$ with respect to 4 cases, as depicted in Fig 3.2(c), are associated to the underlying assumptions.

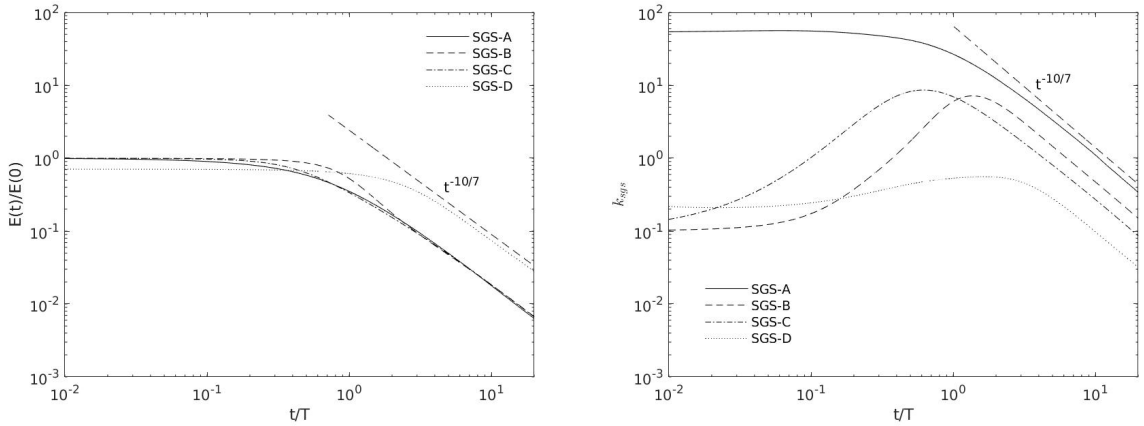

(a) (b)

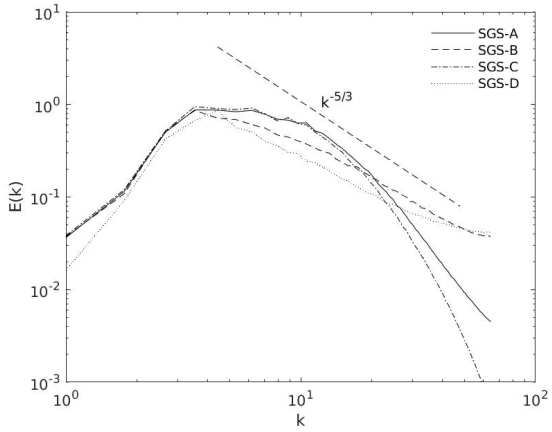

(c)

Figure 3.2: A comparison of the second moment of the velocity field with respect to 4 subgrid models, Kolmogorov's decay law $t^{-10/7}$, and power law, $k^{-5/3}$. (a) $E(t)/E(0)$ and $t^{-10/7}$. (b) k_{sgs} and $t^{-10/7}$. (c) $E(k)$ at $t/T = 3$ and $k^{-5/3}$.

3.4.2.1 Viscous dissipation

In an incompressible fluid, the viscous dissipation $\epsilon = 2\nu\mathcal{S}_{ij}\mathcal{S}_{ij}$ represents the rate of a loss of kinetic energy by the viscous deformational work done by a turbulent flow. It can also be shown that $\langle\epsilon\rangle \equiv 2\nu\langle\mathcal{S}_{ij}\mathcal{S}_{ij}\rangle = \nu\langle\omega_i\omega_i\rangle$. Subfilter scale turbulence stresses τ_{ij} perform the deformational work. Turbulence energy production $-\tau_{ij}\mathcal{S}_{ij}$ is always positive for eddy viscosity models considered in this study. In other words, the rate of loss of resolved turbulence kinetic energy, dE/dt, is expected to be the same as the rate of turbulence production. Figure 3.3 compares the viscous dissipation and the production of TKE by turbulence among 4 cases. It can be seen that the statistics of the velocity fields $\mathcal{X}$ collected from 4 cases of LES are in a good agreement with the known dynamics of homo-

geneous isotropic turbulence. A close agreement between dE/dt and $-\langle \tau_{ij}\mathcal{S}_{ij}\rangle$ in Figure 3.3a infers that vortex stretching does not oppose the energy dissipation in the present test case.

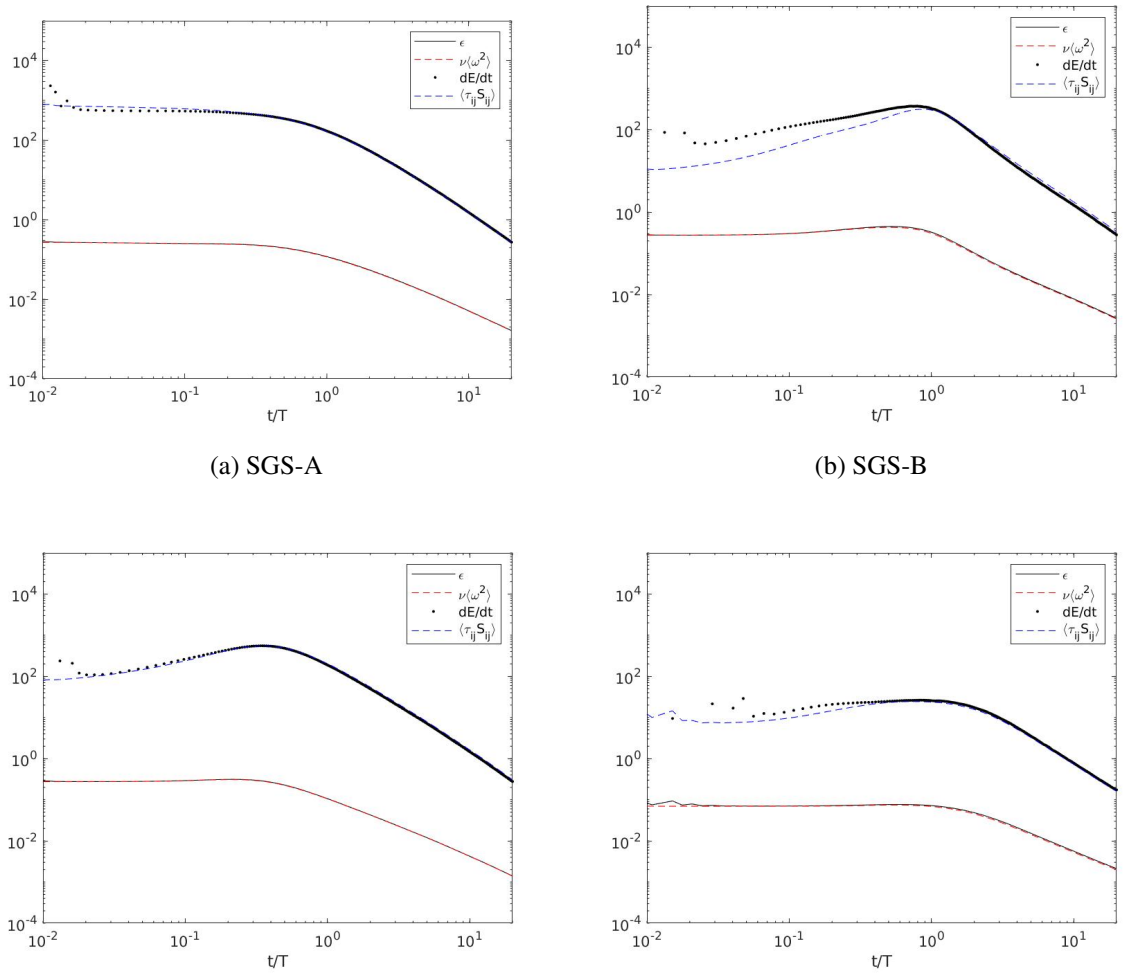

(a) SGS-A

(b) SGS-B

(c) SGS-C

(d) SGS-D

Figure 3.3: A comparison between the time series of the rate of change of the resolved energy, dE/dt, and the energy flux $\langle \tau_{ij}\mathcal{S}_{ij}\rangle$, as well as the viscous dissipation rate ϵ and the mean enstrophy $\langle \omega^2 \rangle$. (a) SGS-A, (b) SGS-B, (c) SGS-C, and (d) SGS-D.

3.4.3 Joint probability distribution

To capture the subtle balance between transport and dissipation in turbulent flows, LES needs to be frame invariant. Thus, subgrid models are typically derived from some functional of invariants of the velocity gradient tensor $\partial \bar{u}_i/\partial x_j$. A dynamical relationship between the principal invariants of $\partial \bar{u}_i/\partial x_j$ maybe written as a dynamical system:

$$\frac{dQ_G}{dt} = -3R_G; \ \frac{dR_G}{dt} = \frac{2}{3}Q_G^2;$$

$$\frac{dQ_S}{dt} = -2R_S - R_G; \quad \frac{dR_S}{dt} = \frac{2}{3}Q_G Q_S + \frac{1}{4}\mathcal{V}^2;$$
$$\frac{d\mathcal{V}^2}{dt} = -\frac{16}{3}(R_S - R_G)Q_G.$$

As discussed earlier, Q and R denote the second and third invariants, respectively, of a tensor. The subscript G or S indicates that the corresponding tensor is either the velocity gradient ($\mathcal{G}$) or the strain rate ($\mathcal{S}$). For brevity, the magnitude of the vortex stretching vector is denoted by $\mathcal{V} = |\mathcal{S}\boldsymbol{\omega}|$. It can be seen that the first two of the system of equations are not dependent on the remaining three equations. Also, each invariants are evaluated on a set of $\mathcal{N}$ grid points. Recall that $\mathcal{N} = 128^3$ for the present analysis.

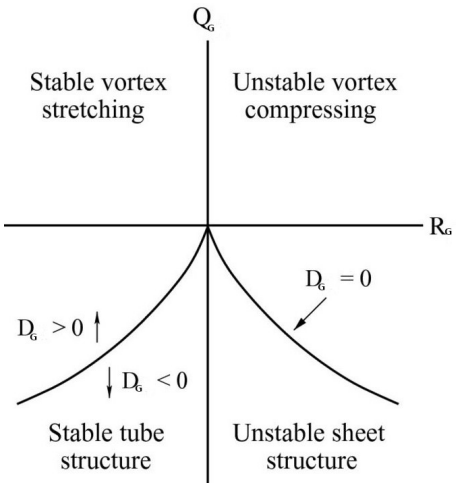

Figure 3.4: The joint probability density function of Q and R for the velocity gradient tensor $\mathcal{G}$, indicating the line defined by $D = (27/4)R^2 + Q^3$.

To understand the phase-portrait corresponding to such a high-dimensional dynamical system (*e.g.* $\mathcal{N} = 128^3$), we consider the joint probability distribution (JPDF) for a pair of invariants. Figure 3.4 schematically indicates the JPDF of the first two equations of the system. Additional mathematical analysis of such invariants are given by (da Silva & Pereira, 2008) and (Trias et al., 2015).

Fig. 3.5 compares the JPDFs of two invariants R_G and Q_G among 4 subgrid models. If $Q_G > 0$, then the production of enstrophy dominates over the production of strain. An interpretation of R_G with respect to the positive and the negative values of Q_G is depicted in Fig. 3.4. In Fig. 3.5, two important characteristics of the JPDF of Q_G and R_G are observed. First, a trend of the teardrop shape is seen in the phase diagram of Q_G and R_G, which suggests that the total strain $\mathcal{S}_{ij}\mathcal{S}_{ij}$ increases, see (Chacín et al., 1996; Elsinga & Marusic, 2010; Ooi et al., 1999; Dallas & Alexakis, 2013). Second, the bulk of the data appears in the upper-left quadrant, where the vortex stretching is positive,

$\omega_i\omega_j\mathcal{S}_{ij} > 0$. The similarity of the invariant map (R_G, Q_G) with respect to 4 subgrid models, as shown in Fig 3.5, demonstrates that both $\omega_i\omega_j\mathcal{S}_{ij}$ and $\mathcal{S}_{ij}\mathcal{S}_{ij}$ play a role in the energy cascade through nonlinear interactions of turbulence structures.

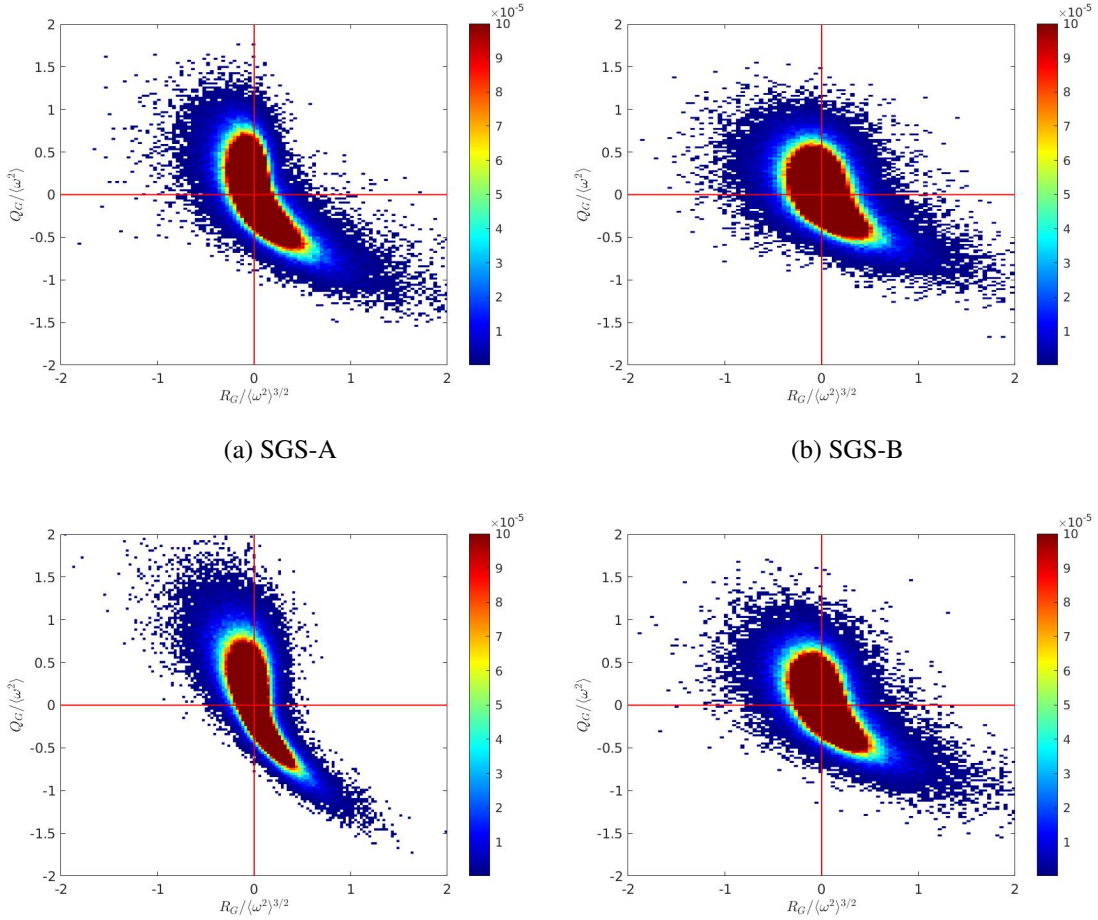

(a) SGS-A

(b) SGS-B

(c) SGS-C

(d) SGS-D

Figure 3.5: The plots of the joint probability density function of two invariants Q_G and R_G of the velocity gradient tensor $\mathcal{G}$.

Similarly, Fig. 3.6 compares the invariant map of Q_S and R_S corresponding to 4 subgrid models, where a strong preference for the zone, $R_S > 0, Q_S < 0$, is observed. The (R_S, Q_S) map indicates the region ($R_S > 0, Q_S < 0$) of intense kinetic energy dissipation, as it is observed in many turbulent flows, *e.g.* see (Ooi et al., 1999; da Silva & Pereira, 2008).

The correlation between the second invariants of the rotation tensor $\mathcal{R}_{ij}$ and that of the strain tensor $\mathcal{S}_{ij}$ is shown in Fig. 3.7. The invariant map (Q_S, Q_R) indicates a strong correlation between dissipation and enstrophy along the diagonal of the map $Q_S = Q_R$.

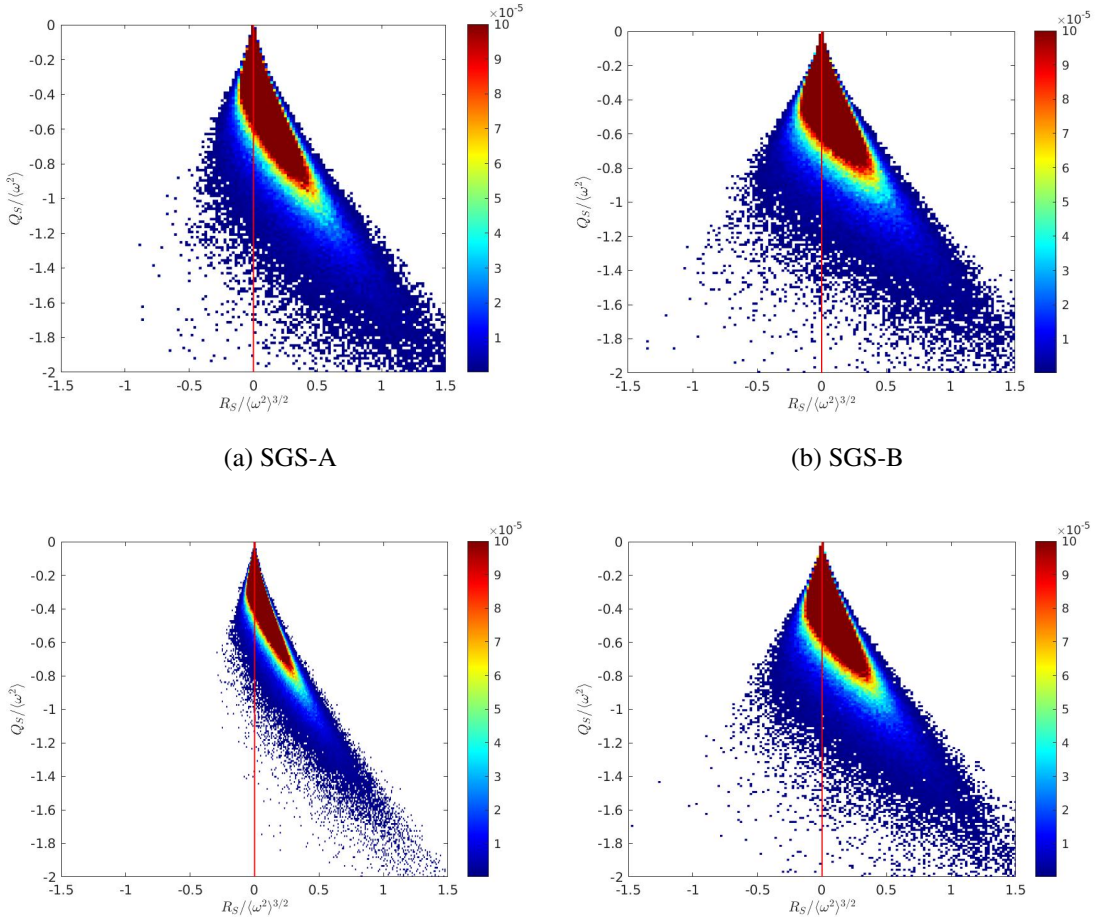

(a) SGS-A

(b) SGS-B

(c) SGS-C

(d) SGS-D

Figure 3.6: The plots of the joint probability density function of two invariants R_S and Q_S of the strain rate tensor $\mathcal{S}$.

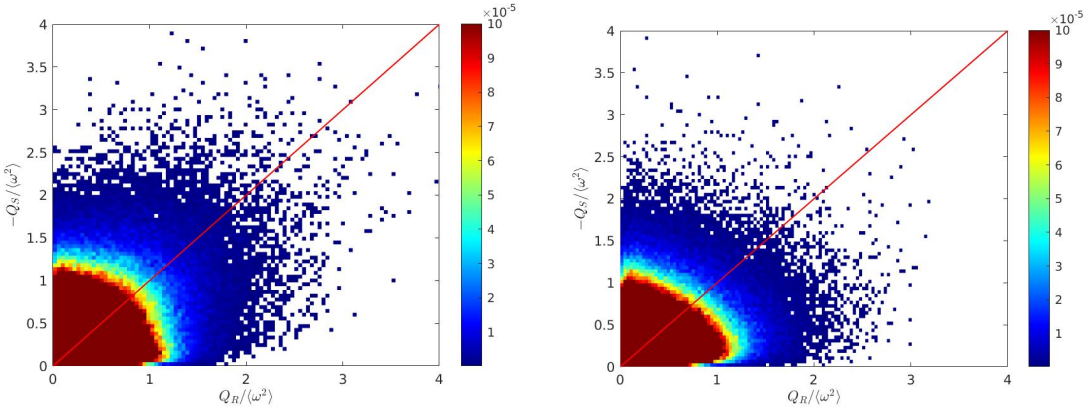

(a) SGS-A (b) SGS-B

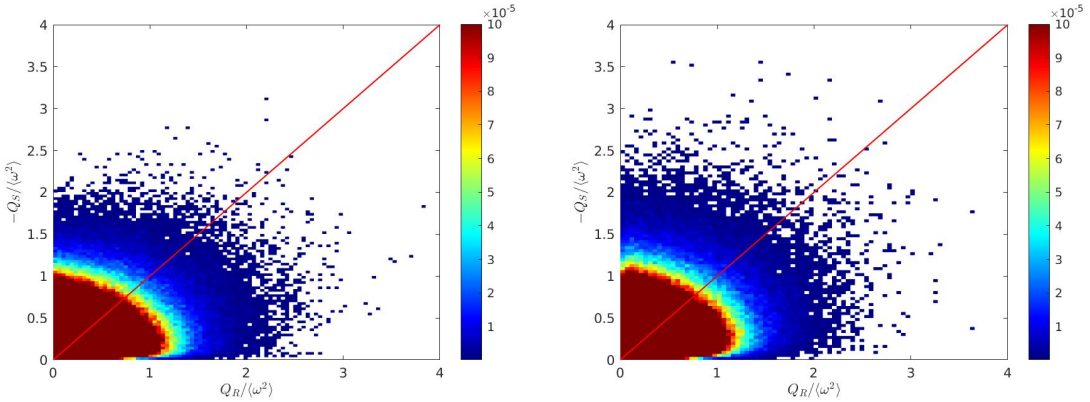

(c) SGS-C (d) SGS-D

Figure 3.7: The plots of the joint probability density function of the second invariant Q_S and Q_R of two tensors $\mathcal{S}$ and $\mathcal{R}$, respectively.

3.5 Conclusion

In this article, we study the subgrid-scale dissipation and the turbulence production in turbulent flows. The brief analysis of JPDFs suggests that the stretching of vortex tubes and filaments is a primary mechanical cause of dissipation in turbulent motion. Considering the square of the velocity gradient tensor in the eddy viscosity model indicates that the diffusion of the vorticity is relevant in subgrid-scale energy dissipation. The study also observes that a turbulence model can learn about the rate of subgrid-scale dissipation, *e.g.*, from singular values of the velocity gradient tensor, even when the flow structures are marginally resolved (*e.g.* Table 3.1). Although the study is limited to decaying turbulence, the findings lay the framework for a potentially novel machine learning approach for subgrid model, which may be further advanced.

Chapter 4

Conclusion

The present thesis focuses on the modeling of the subgrid-scale dissipation rate and the production of turbulence in turbulent flows. Following this idea, the statistics of the velocity gradient tensor are used to estimate the subgrid-scale dissipation rate and validate the statistical analysis among the four subgrid-scale models, such as SGS-A, SGS-B, SGS-C, and SGS-D. The SGS-A model is considered a vortex-stretching-based model based on the square of the velocity gradient tensor. In this model, the vortex stretching mechanism helps to estimate the energy dissipation rate and characterizes the energy cascade of turbulent flows. The performance of the SGS-A model is compared with the other three subgrid-scale models (SGS-B, SGS-C, and SGS-D) by using *a posteriori* statistics of LES data and joint probability density function of the velocity gradient tensor. When four subgrid-scale models are compared, it is found that the SGS-A model accounts for more subgrid-scale energy than other subgrid-scale models.

4.1 Summary of findings

Some interesting findings of the four subgrid-scale models are listed here sequentially:

- The behavior of the velocity gradient skewness is used to confirm the development of turbulence. The value of derivative skewness originates from close to zero and decreases and increases at a certain level. After some eddy turn-over time ($t/T > 0.1$), the skewness of the velocity gradient of the subgrid-scale models stabilized around -0.4, see Fig. 3.1. It suggests that the kinetic energy is transferred to the downscales and is balanced by viscous dissipation in the subgrid-scale models.

- The resolved velocity of turbulent flow is sufficient to predict the subgrid-scale dissipation by using the statistics of the velocity gradient tensor. The first- and higher-order moments of turbulence are found to be robustly consistent with the previous works in the literature. The LES simulations are able to reproduce the statistics from the similarity hypothesis. The energy spectrum of the interested subgrid-scale models has a good profile in the inertial subrange. However, the energy spectrum of SGS-B and SGS-D are not dissipating like SGS-A and SGS-C subgrid models, which may be the reason for the insufficient resolution, see Fig. 3.2(c).

- The decay rate of the time evolution of the resolved kinetic energy is showing $(t - t_0)^{-10/7}$, which indicates that the energy is transferred to the downscales at a constant rate which supports Kolmogorov's decay law, $E(t) \sim (t - t_0)^{-10/7}$, see Fig. 3.2(a). The subgrid-scale model SGS-A agrees with the other three subgrid-scale models by considering the Kolmogorov research in the literature.

- The time evolution of turbulent kinetic energy (k_{sgs}) among the four subgrid-scale models are computed from the trace of the subgrid-scale stress tensor. The k_{sgs} plot indicates that the SGS-A model has captured more energy than the other subgrid-scale models with respect to Kolmogorov's decay law $(t - t_0)^{-10/7}$, see Fig. 3.2(b).

- In the SGS-A model, the loss of turbulence is more correlated to turbulence production than the other three subgrid-scale models. Thus, a close agreement between the production of turbulence and loss of turbulence in the SGS-A model indicates that vortex stretching does not oppose energy dissipation, i.e., vortex stretching cascades energy, see Fig. 3.3.

- In the statistical analysis of JPDF, the (Q_G,R_G) diagram of four subgrid-scale models appear in a teardrop shape, which indicates the similar accuracy of the subgrid-scale models, see Fig. 3.5. A significant portion of the fluid elements is dominated by vortex stretching and total strain in these diagrams. It suggests that the vortex stretching is present in the subgrid-scale models; simultaneously, the total strain represents the viscous dissipation of small scales kinetic energy in the subgrid-scale models. The JPDF of (Q_S,R_S) of four subgrid-scale models show a similar characteristic behaviour. Among the subgrid-scale models, the SGS-C shows a strong correlation between Q_S and R_S, which suggests there is more dissipation in the SGS-C model than other the subgrid-scale models, see Fig. 3.6. The JPDF of (Q_S,Q_R) of four subgrid-scale

models represents a region along the diagonal line $-Q_S = Q_R$, which indicates the correlation between enstrophy and the dissipation rate. However, the SGS-A model has shown a strong correlation between enstrophy and dissipation rate than other subgrid-scale models, see Fig. 3.7.

4.2 Future Work

In this final section, a list of some recommendations for future work is offered.

- These findings suggest that a turbulence model can effectively learn about the subgrid-scale dissipation from singular values of the velocity gradient tensor.
- We may extend the SGS-A model to develop a new model by using other tensors and invariants.
- We can analyze the past history of data and combine other data driving techniques with the vortex stretching mechanism.
- The findings of the JPDF of the invariants of the velocity gradient tensor suggest that we may further learn about the JPDF of the high-resolution LES data.
- Other possible further applications of this study can include:
  - Earth and ocean atmosphere
  - aerodynamics simulations
  - lift-generated by wings
  - fluid-solid interactions
  - magnetohydrodynamic turbulence

References

Afonso, M. M., & Meneveau, C. (2010). Recent fluid deformation closure for velocity gradient tensor dynamics in turbulence: timescale effects and expansions. *Physica D: Nonlinear Phenomena*, *239*(14), 1241–1250.

Alam, J., & Islam, M. R. (2015). A multiscale eddy simulation methodology for the atmospheric ekman boundary layer. *Geophysical & Astrophysical Fluid Dynamics*, *109*(1), 1–20.

Alam, J. M., & Fitzpatrick, L. P. (2018). Large eddy simulation of flow through a periodic array of urban-like obstacles using a canopy stress method. *Computers & Fluids*, *171*, 65–78.

Bernard, P. S., Thangam, S., & Speziale, C. G. (1992). The role of vortex stretching in turbulence modeling. In *Instability, transition, and turbulence* (pp. 563–574). Springer.

Bhuiyan, M. A. S., & Alam, J. M. (2020). Scale-adaptive turbulence modeling for les over complex terrain. *Engineering with Computers*, 1–13.

Bradshaw, P. (1997). Understanding and prediction of turbulent flow1996. *International journal of heat and fluid flow*, *18*(1), 45–54.

Buxton, O. R., Breda, M., & Chen, X. (2017). Invariants of the velocity-gradient tensor in a spatially developing inhomogeneous turbulent flow. *Journal of Fluid Mechanics*, *817*, 1–20.

Carbone, M., & Bragg, A. D. (2020). Is vortex stretching the main cause of the turbulent energy cascade? *Journal of Fluid Mechanics*, *883*.

Chacín, J. M., Cantwell, B. J., & Kline, S. J. (1996). Study of turbulent boundary layer structure using the invariants of the velocity gradient tensor. *Experimental thermal and fluid science*, *13*(4), 308–317.

Dallas, V., & Alexakis, A. (2013). Structures and dynamics of small scales in decaying magnetohydrodynamic turbulence. *Physics of Fluids*, *25*(10), 105106.

da Silva, C. B., & Pereira, J. C. (2008). Invariants of the velocity-gradient, rate-of-strain, and rate-of-rotation tensors across the turbulent/nonturbulent interface in jets. *Physics of fluids*, *20*(5),

055101.

Davidson, P. (2004). *Turbulence: an introduction for scientists and engineers.* Oxford University Press.

Deardorff, J. W. (1972). Numerical investigation of nutral and unstable planetary boundary layer. *J. Atmospheric Science*, *29*, 91-115.

Deardorff, J. W., et al. (1970). A numerical study of three-dimensional turbulent channel flow at large reynolds numbers. *J. Fluid Mech*, *41*(2), 453–480.

Elsinga, G., & Marusic, I. (2010). Universal aspects of small-scale motions in turbulence. *Journal of Fluid Mechanics*, *662*(514-539), 20.

Fureby, C., Tabor, G., Weller, H., & Gosman, A. (1997). A comparative study of subgrid scale models in homogeneous isotropic turbulence. *Physics of fluids*, *9*(5), 1416–1429.

Hirota, M., Nishio, Y., Izawa, S., & Fukunishi, Y. (2017). Vortex stretching in a homogeneous isotropic turbulence. In *Journal of physics: Conference series* (Vol. 822, p. 012041).

Kevlahan, N.-R., Alam, J., & Vasilyev, O. V. (2007). Scaling of space–time modes with reynolds number in two-dimensional turbulence. *Journal of Fluid Mechanics*, *570*, 217–226.

Kim, W.-W., & Menon, S. (1995). A new dynamic one-equation subgrid-scale model for large eddy simulations. In *33rd aerospace sciences meeting and exhibit* (p. 356).

Kolmogorov, A. N. (1941). On degeneration (decay) of isotropic turbulence in an incompressible viscous liquid. In *Dokl. akad. nauk sssr* (Vol. 31, pp. 538–540).

Kolmogorov, A. N. (1962). A refinement of previous hypotheses concerning the local structure of turbulence in a viscous incompressible fluid at high reynolds number. *Journal of Fluid Mechanics*, *13*(1), 8285. doi: 10.1017/S0022112062000518

Kundu, P. K., Cohen, I. M., & Dowling, D. (2008). *Fluid mechanics 4th.* Elsevier.

Leonard, A., & Peters, N. (2011). Theodore von kármán. *This page intentionally left blank*, 101.

Lesieur, M., Métais, O., Comte, P., et al. (2005). *Large-eddy simulations of turbulence*. Cambridge university press.

Lilly, D. K. (1992). A proposed modification of the germano subgrid-scale closure method. *Physics of Fluids A: Fluid Dynamics*, *4*(3), 633–635.

Lund, T. S., & Novikov, E. (1992). Parameterization of subgrid-scale stress by the velocity gradient tensor. *Annual Research Briefs*, *1992*, 27–43.

Lundgren, T. S. (2003). *Linearly forces isotropic turbulence* (Tech. Rep.). MINNESOTA UNIV MINNEAPOLIS.

Martín, J., & Dopazo, C. (1995). Velocity gradient invariant evolution from a linear diffusion model. In *Proc. twelfth australasian fluid mechanics conf* (pp. 743–746).

Martın, J., Ooi, A., Chong, M. S., & Soria, J. (1998). Dynamics of the velocity gradient tensor invariants in isotropic turbulence. *Physics of Fluids*, *10*(9), 2336–2346.

Meneveau, C. (2010). Turbulence: Subgrid-scale modeling. *Scholarpedia*, *5*(1), 9489.

Meneveau, C., Lund, T. S., & Cabot, W. H. (1996). A lagrangian dynamic subgrid-scale model of turbulence. *Journal of fluid mechanics*, *319*, 353–385.

Nicoud, F., & Ducros, F. (1999). Subgrid-scale stress modelling based on the square of the velocity gradient tensor. *Flow, turbulence and Combustion*, *62*(3), 183–200.

Onsager, L. (1949). Statistical hydrodynamics. *Il Nuovo Cimento (1943-1954)*, *6*(2), 279–287.

Ooi, A., Martin, J., Soria, J., & Chong, M. S. (1999). A study of the evolution and characteristics of the invariants of the velocity-gradient tensor in isotropic turbulence. *Journal of Fluid Mechanics*, *381*, 141–174.

Pletcher, R. H., Tannehill, J. C., & Anderson, D. (2012). *Computational fluid mechanics and heat transfer*. CRC press.

Pope, S. B. (2001). *Turbulent flows*. IOP Publishing.

Reynolds, O. (1883). Xxix. an experimental investigation of the circumstances which determine whether the motion of water shall be direct or sinuous, and of the law of resistance in parallel channels. *Philosophical Transactions of the Royal society of London*(174), 935–982.

Richardson, L. F. (2007). *Weather prediction by numerical process*. Cambridge university press.

Rosales, C., & Meneveau, C. (2005). Linear forcing in numerical simulations of isotropic turbulence: Physical space implementations and convergence properties. *Physics of fluids*, *17*(9), 095106.

Sagaut, P. (2006). *Large eddy simulation for incompressible flows: an introduction*. Springer Science & Business Media.

Sagaut, P., & Cambon, C. (2008). *Homogeneous turbulence dynamics* (Vol. 10). Springer.

Shetty, D. A., & Frankel, S. H. (2013). Assessment of stretched vortex subgrid-scale models for les of incompressible inhomogeneous turbulent flow. *International journal for numerical methods in fluids*, *73*(2), 152–171.

Smagorinsky, J. (1963). General circulation experiments with the primitive equations: I. the basic experiment. *Monthly weather review*, *91*(3), 99–164.

Storer, L. N., Williams, P. D., & Gill, P. G. (2019). Aviation turbulence: dynamics, forecasting, and response to climate change. *Pure and Applied Geophysics*, *176*(5), 2081–2095.

Taylor, G. I. (1932). The transport of vorticity and heat through fluids in turbulent motion. *Proceedings of the Royal Society of London. Series A, Containing Papers of a Mathematical and Physical Character*, *135*(828), 685–702.

Taylor, G. I. (1938). Production and dissipation of vorticity in a turbulent fluid. *Proceedings of the Royal Society of London. Series A-Mathematical and Physical Sciences*, *164*(916), 15–23.

Tennekes, H., & Lumley, J. L. (2018). *A first course in turbulence*. MIT press.

Trias, F., Folch, D., Gorobets, A., & Oliva, A. (2015). Building proper invariants for eddy-viscosity subgrid-scale models. *Physics of Fluids*, *27*(6), 065103.

Verzicco, R., Fatica, M., Iaccarino, G., Moin, P., & Khalighi, B. (2002). Large eddy simulation of a road vehicle with drag-reduction devices. *AIAA journal*, *40*(12), 2447–2455.

Wilcox, D. C., et al. (1998). *Turbulence modeling for cfd* (Vol. 2). DCW industries La Canada, CA.

Yoshizawa, A. (1986a). Statistical theory for compressible turbulent shear flows, with the application to subgrid modeling. *The Physics of fluids*, *29*(7), 2152–2164.

Yoshizawa, A. (1986b). Statistical theory for compressible turbulent shear flows, with the application to subgrid modeling. *The Physics of Fluids*, *29*(7), 2152-2164.